Geological Quarterly, 2025, 69, 19
DOI: https://doi.org/10.7306/gq.1792

Newly found tuffic horizons in the Visean deposits of the Lublin Basin, SE Poland: petrological characteristics, origin and stratigraphic significance

Aleksandra KOZŁOWSKA[1, *], Maria I. WAKSMUNDZKA[1] and Marek SZCZERBA[2]

[1] Polish Geological Institute-National Research Institute, Rakowiecka 4, 00-975 Warszawa, Poland; ORCID: 0000-0002-6360-4974 [A.K.], 0000-0001-8554-7766 [M.W]

[2] Institute of Geological Sciences, Polish Academy of Sciences – Research Centre in Kraków, Senacka 1, 31-002 Kraków, Poland; ORCID: 0000-0002-0485-886X

Kozłowska, A., Waksmundzka, M.I., Szczerba, M., 2025. Newly found tuffic horizons in the Visean deposits of the Lublin Basin, SE Poland: petrological characteristics, origin and stratigraphic significance. Geological Quarterly, 69, 19; https://doi.org/10.7306/gq.1792

Associate Editor: Anna Wysocka

Detailed petrographical and mineralogical analyses are provided of tuffic horizons identified for the first time in Upper Visean deposits (sequences 2 and 3) in 21 boreholes of the Lublin Basin, along with co-occurring volcaniclastic rocks. The thickness of the tuff horizons varies in the range of 0.2–8 m. Tuff 2.I reaches its maximum thickness in the NE region, and tuffs 2.II and 3.I in the centre of the basin. As these tuffs can be traced between different parts of the basin, they provide good regional correlative horizons. Tuff horizons 2.I and 2.II have been identified within sequence 2, and tuff horizon 3.I in sequence 3. The rhyolitic pyroclastic material composing the tuffs was sourced from the eruptive acidic volcanism that took place in the Lublin Basin in the Late Visean. The pyroclastic material was deposited in various environments that co-occurred in the basin area at that time: fluvial floodplain, deltaic plain, shallow-water delta, shallow clay-dominated shelf, and carbonate shelf. Within the horizons studied, fine-ash vitric and vitric-crystal tuffs, and coarse-ash vitric and vitric-lithic tuffs have been identified. The main clay mineral in the tuffs is kaolinite, the content of which can exceed 80%. In some areas it is accompanied by serpentine – berthierine, whereas in others, mixed-layered illite/smectite minerals and illite predominate. Anatase and carbonate minerals of siderite, sideroplesite and Fe/Mn-calcite are common. Hematite, pyrite and jarosite are also sometimes found. The recent composition of the tuffs results mainly from the type of pyroclastic material, as well as from the factors it has been subjected to, including sedimentary environment, hypergenic weathering, and hydrothermal and diagenetic processes. The detrital components found in the volcaniclastic conglomerates and sandstones were derived mostly from erosion and reworking of rocks from sequences 1 and 2 occurring within the sedimentary basin, and to a lesser extent they came from outside of the basin. Preliminary mineral resource studies have shown that the tuffic horizons can contain ~28-35% of Al_2O_3, which is a prospective quantity for refractory raw materials. The volcaniclastic rocks, in which enrichment in rare earth elements is found, also show the potential for being economic raw materials. The conclusions about the raw material potential should be considered preliminary, requiring further research.

Key words: tuffs, volcaniclastic rocks, clay minerals, correlation horizons, Visean, Lublin Basin.

INTRODUCTION

In the Lublin Basin (Fig. 1), deposits admixed with pyroclastic material were first described by Cebulak and Porzycki (1966), from Devonian-Carboniferous boundary strata. Later, they were distinguished along with co-occurring volcanic rocks by Żelichowski (1969, 1972) as the Kłodnica Member within the Huczwa Formation (Fig. 2). Descriptions of these rocks can be found in an archival study (Jackowicz, 1985) and in publications (Depciuch, 1974; Popek, 1986; Cebulak, 1988a, b; Porzycki, 1988; Grocholski and Ryka, 1995; Porzycki and Zdanowski, 1995). Over the next few years, these rocks remained out of research focus. Recently, petrographic and stratigraphic studies of rocks containing volcanic material have resumed (Kozłowska and Popek, 2018; Kozłowska and Waksmundzka, 2020, 2023; Waksmundzka et al., 2021). They showed that the Kłodnica Member deposits span both the oldest rocks in the Carboniferous succession, presumably of Tournaisian age, and Visean rocks, separated by a stratigraphic gap (Figs. 2 and 3). The work resulted in the identification of new correlative tuffic horizons in the Lublin Basin, as well as of the inferred location of volcanic cones active in Visean times. These pyroclastic layers demonstrate that palaeovolcanism took place, and are the basis for its interpretation given the absence of effusive volcanic

* Corresponding author, e-mail: aleksandra.kozlowska@pgi.gov.pl

Received: May 9, 2024; accepted: June 7, 2025; first published online: August 1, 2025

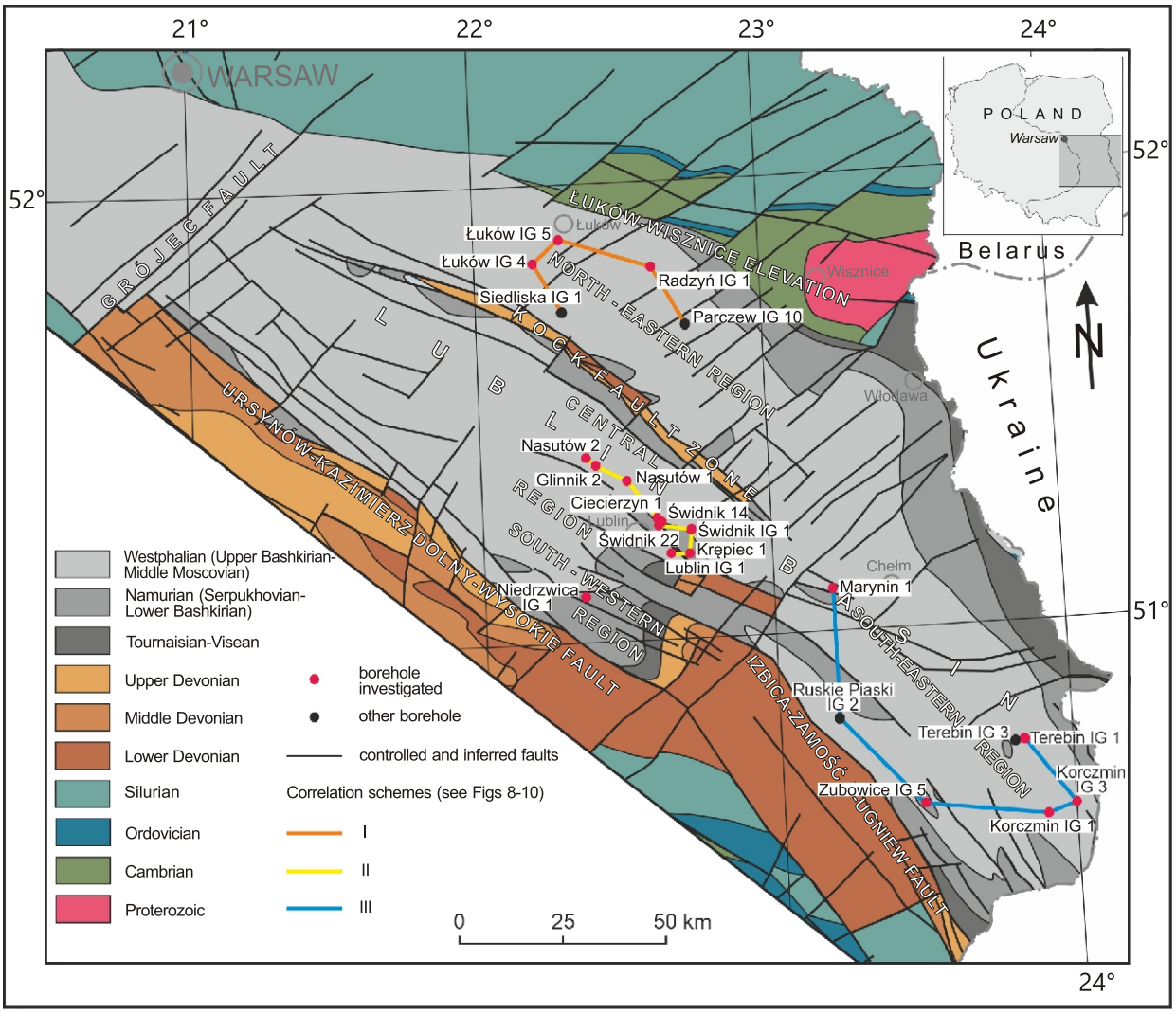

Fig. 1. Geological-structural map of the Lublin Basin without strata younger than Carboniferous (modified after Waksmundzka and Buła, 2020), with location of the boreholes studied

rocks in the Visean formations studied. Such volcanic rocks have been recognised in sequence 1 strata (Waksmundzka et al., 2021) and are Tournaisian in age (Pańczyk and Nawrocki, 2015). Mississippian (mainly Tournaisian) volcanism is also known in the Western Pomerania (Muszyński et al.,1996) and the Holy Cross Mountains (Migaszewski, 1995; Krzemiński, 1999).

This paper provides details on the petrography and mineralogy of these newly identified tuffic horizons together with co-occurring volcaniclastic rocks within the Visean deposits. The results are tied to the results of sedimentological and sequence stratigraphic studies to reconstruct the origin of the deposits, as well as their spatial and age relationships. These horizons are younger than the previously described tuffs from sequence 1, which are of Tournaisian age, as they occur within the Visean sequences of 2 and 3. So far, only two tuffs of this age have been previously described from the NE part of the basin: one in the Siedliska IG 1 borehole (Kozłowska and Popek, 2018) and the other in the Radzyń IG 1 borehole (Waksmundzka et al., 2021). The question of their regional nature and possible correlations, based on a larger number of borehole sections from various parts of the basin, is important to understanding the regional geology.

GEOLOGICAL SETTING

The Lublin Basin (Fig. 1) covers an area of Carboniferous subcrops at the basal surface of the Permian-Mesozoic succession in SE Poland. Its continuation is the Lviv-Volhynia Basin, located in Ukraine. The Lublin Basin is a segment of the newly defined Carboniferous Płock-Lublin Basin (Narkiewicz, 2023). It is separated from the Płock segment by the Grójec Fault. The basin is filled with Upper Tournaisian-Upper Moscovian deposits (Fig. 2), separated from various Devonian, lower Paleozoic and Ediacaran formations, as well as from crystalline basement rocks, by a stratigraphic gap (Cebulak, 1988b). The deposition of Carboniferous rocks was preceded by an erosion event lasting in this area through the Early and Middle Tournaisian (Waksmundzka et al., 2021), and in some areas continuing into the Middle Visean (Waksmundzka, 2010). There is a distinct unconformity and a stratigraphic gap at the top of the Carboniferous section, associated with the Variscan orogeny (Narkiewicz, 2023). The overlying Upper Permian deposits represent the Polish Zechstein Basin (Peryt, 2023), followed by rocks of the Mesozoic Basin of the Polish Lowlands (Leszczyński, 2023), the Paleogene-Neogene Basin of the Polish Lowlands (Kasiński, 2023), and the youngest, Quaternary deposits.

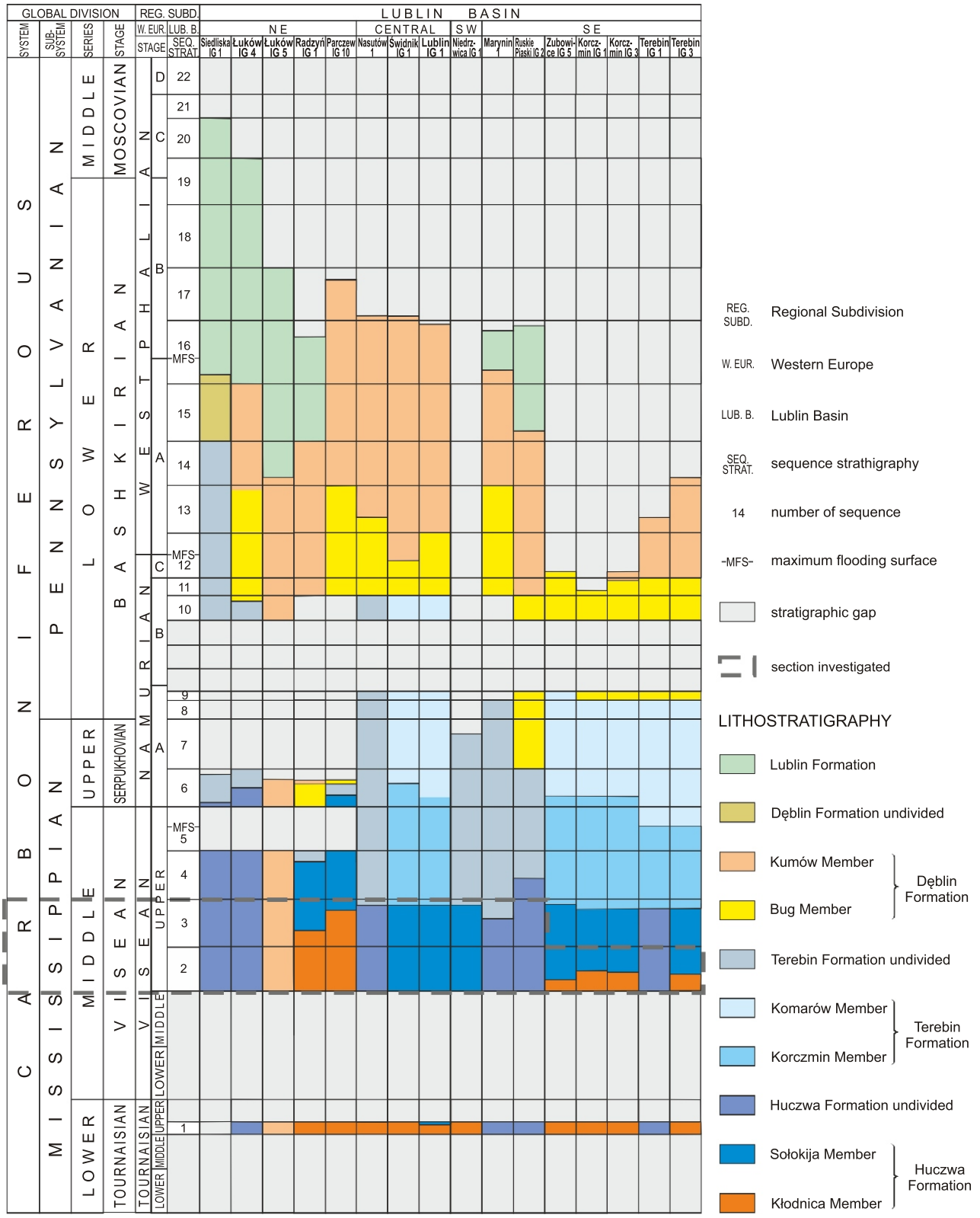

Fig. 2. Chronostratigraphic divisions, lithostratigraphy and sequence stratigraphy of the Carboniferous succession in some of the boreholes studied

According to informal lithostratigraphic division (Porzycki and Żelichowski, 1977, *fide* Porzycki, 1979), the oldest part of the Carboniferous section represents the Huczwa Formation subdivided into the Kłodnica and Sołokija members (Fig. 2). The age of these deposits was constrained to the Upper Visean, based on biostratigraphic studies (Musiał and Tabor, 1979, 1988; Porzycki and Zdanowski, 1995). However, the latest results of sequence stratigraphic studies by Waksmundzka et al. (2021) indicate an earlier onset of Carboniferous deposition, presumably in the Late Tournaisian. It was also found that the boundaries of the Kłodnica Member are diachronous and its time span is variable and differs from region to region in the basin. To the NE, the Kłodnica Member encompasses sequences 1–3, and sequences 1–2 in the rest of the area. The age of sequence 1 has been assigned to the Upper Tournaisian, and of sequences 2–3 to the Upper Visean (Waksmundzka et al., 2021). The age of sequences 2–3 was based on many biostratigraphic studies of faunal (Musiał and Tabor, 1979, 1988; Skompski and Soboń-Podgórska, 1980; Soboń-Podgórska 1988; Soboń-Podgórska and Tomaś, 1995; Skompski 1996) and floral (Migier, 1988; Kmiecik, 1988) remains.

In the study area, the Kłodnica Member is ~10–37 m thick, the greatest thickness being recorded in the NE region in the Parczew IG 10 borehole, in the central region in Świdnik IG 1, and in the SW region in Niedrzwica IG 1. In the NE region, the unit is represented by claystones, mudstones, volcaniclastic sandstones and conglomerates, limestones, tuffs, bauxites and basalts. Similar rocks are found in the central and SW regions, with the exception of limestones and bauxites. In the SE, its lithology is the least diverse and consists of mudstones, sandstones, conglomerates, tuffs and, in a single section, altered volcanic rocks.

Previous radiometric dating of the Kłodnica Member volcanic rocks indicate a Namurian and Late or Middle Visean age of their formation (Depciuch, 1974). Porzycki (1988) and Grocholski and Ryka (1995) inferred a Late Visean age for this member. Recent dating (by the $^{40}Ar/^{39}Ar$ method) of basalts from the NE part of the basin indicates they are older, corresponding to the Upper Tournaisian (Pańczyk and Nawrocki, 2015). Tomaszczyk and Jarosiński (2017) suggested that volcanic activity in the Tournaisian occurred under extensional conditions, whereas in the Visean, there was an evolution of the stress regime from compressional to extensional. According to Narkiewicz (2007), Early Carboniferous volcanic activity should be associated with a hot spot.

The Kłodnica Member is overlain by deposits of the upper part of the Huczwa Formation, representing the Sołokija Member dominated by claystones, mudstones, marls and limestones, containing a marine fauna. *Stigmaria* soil horizons and thin coal layers have been encountered in the claystones. The maximum thickness of the Sołokija Member, ~400 m, is found in the SW region. In the central and SE regions, it may be ~150–200 m thick.

MATERIAL AND METHODS

The sedimentological and sequence stratigraphic studies were based on geological and geophysical data from 21 boreholes shown in Figure 1 and located in the NE, SW, central and SE regions of the Lublin Basin. Among these boreholes, eight sections (Ciecierzyn 1, Glinnik 2, Łuków IG 4, Łuków IG 5, Krępiec 1, Świdnik 14, Świdnik 22) were subjected to a full lithofacies-stratigraphic analysis. New tuffic horizons, so far unknown, were identified in eight previously studied boreholes (Korczmin IG 1, Korczmin IG 3, Lublin IG 1, Marynin 1, Nasutów 1, Świdnik IG 1, Terebin IG 1, Terebin IG 3) (Waksmundzka, 2010, 2018; Kozłowska and Waksmundzka, 2020; Waksmundzka et al., 2021). The remaining sections were used to correlate and portray the regional lithofacies pattern of the deposits under study. Eight of the boreholes (Łuków IG 4, Łuków IG 5, Radzyń IG 1, Parczew IG 10, Marynin 1, Korczmin IG 1, Korczmin IG 3) provide completely cored sections, while the others are cored in part. Five of the boreholes (Korczmin IG 3, Nasutów 1, Nasutów 2, Świdnik 22, Terebin IG 1) provide long cored intervals, several tens of metres thick, which facilitated the detailed study of tuffic horizons found within them.

The sedimentological studies were based on lithofacies analysis. Individual lithofacies (Reading, 1978; Walker, 1992) were separated and coded using a lithofacies coding system (after Miall, 1977, 1978; Rust, 1978; Zieliński, 1992a, b, 1995; Waksmundzka, 2012, 2013). Each lithofacies was assigned to a lithofacies assemblage, corresponding to coarsening-upwards, non-gradational, and fining-upwards cyclothems, using the authors' classification (Waksmundzka, 2013; Kozłowska and Waksmundzka, 2020; Waksmundzka et al., 2021). The original (decompacted) thickness of tuff and sandstone lithofacies (after Baldwin and Butler, 1985) was reconstructed, using a methodology previously tested in sedimentological studies of Carboniferous deposits (Waksmundzka, 2013; Waksmundzka et al., 2021).

Our paper deals with sequences 2 and 3 from the NE and central regions of the Lublin Basin, and sequence 2 from the SE region, in which new, so far unidentified tuffic horizons have been found. Facies development of the deposits of these sequences, the spatial and age relationships within them, and, in particular, the lateral distribution of the tuffic horizons and accompanying volcaniclastic rocks are characterized based on lithological and facies correlations, as well as on sequence stratigraphic data. The following three correlation schemes (Fig. 1) have been constructed using, as a reference level, both the tops of river channel sandstones and the corresponding maximum regression surfaces – initial transgression surfaces.

In the study, we used the sequence stratigraphic subdivision introduced by Waksmundzka (2008, 2010, 2012, 2013) and Waksmundzka et al. (2021) for Carboniferous deposits of the Lublin Basin, using the methodology characterized in detail in her previous studies. The depositional sequences (after Michum, 1977) identified are bounded by type I unconformities (Vail and Todd, 1981). The maximum regression surface – initial transgression surface (T), as well as the maximum flooding surface (MFS) occur within the sequences. They separate (1) a forced-regressive systems tract (FRST), (2) a transgressive systems tract (TST), and (3) a normal-regressive (NR) systems tract, which formed during the highstand (HST) or lowstand (LST) of relative sea level (RSL). The systems tracts consist of parasequences (Van Wagoner, 1985), corresponding to coarsening-upwards, non-gradational and fining-upwards cyclothems.

Thirty-four samples of selected rocks were analysed microscopically using a *Nikon Optiphot 2* polarizing microscope. Thin sections, containing carbonate minerals, were stained with Evamy's solution for their identification. Ten rock samples were subjected to cathodoluminescence (CL) analysis using a cold cathode, model CITL MK5 equipped with EDX, from Cambridge Image Technology Ltd. Scanning electron microscopy (SEM) studies were carried out on a *LEO 1430* type microscope equipped with an EDS ISIS energy microprobe from Oxford Instruments. The conditions for microprobe measurements were: accelerating voltage – 20 kv and beam current – 80 μA. Three chips of rocks and 11 thin sections were examined for chemical analysis of the following minerals: carbonates – 32, clay miner-

als – 9, and anatase – 7. SEM *Quant* software was used for quantitative X-ray analysis when examining the microareas. X-ray diffraction (XRD) studies were carried out on 10 samples using a Bruker D8 X-ray diffractometer, with a Co lamp, equipped with a Vantec-1 high-speed detector. Each sample was crushed gently to sieve through a 0.4 sieve, and then milled with methanol in a McCrone micronising mill. Random orientation of powder specimens was achieved by side-loading. Quantitative mineralogical analysis was performed by fitting the diffractograms of the samples studied using diffractograms of previously recorded pure standards using a QMIN computer program. The accuracy of quantitative XRD analysis largely depends on the crystallinity of the phases studied. For example, phases such as pyrite or anatase can be detected at concentrations below 1%, while for clay minerals, this threshold is around 3%. Additionally, kaolinite crystallinity was evaluated based on X-ray diffraction data using the Hinckley index (HI) (Hinckley, 1963).

The Al_2O_3 content in the rock was estimated (calculated) based on the % kaolinite content obtained from the XRD analysis, assuming, based on published data of Bolewski (1982), the average Al_2O_3 content in kaolinite is equal to 65%.

In this study, we use the general term for the group of volcaniclastic rocks, which refers to clastic rocks containing pyroclastic material, without providing a more specific volume proportion (after Ryka and Maliszewska, 1991). This group of rocks comprises tuffs, which contain >75% of pyroclastic material, and volcaniclastic conglomerates, sandstones and mudstones consisting of pyroclastic and epiclastic material in variable proportions. Classification of pyroclastic rocks is based on type and size of material (Le Maitre et al., 2002). The nomenclature of sandstones is based on the modified classification by Pettijon et al. (1972), and of conglomerates, by Jaworowski (1987) and Ryka and Maliszewska (1991).

RESULTS

SEDIMENTOLOGICAL ANALYSIS AND SEQUENCE STRATIGRAPHY

LITHOFACIES AND CYCLICITY

In sequences 2 and 3, the most common rocks in terms of thickness are claystones and mudstones interbedded with limestones. Volcaniclastic sandstones, mainly fine-grained, are relatively common, while medium- to coarse-grained sandstones and volcaniclastic conglomerates are less frequent.

Humic coals and carbonaceous claystones are rare and occur as interbeds within the claystone-mudstone intervals. The lithofacies analysis of cored sections enabled the distinguishing of a number of lithofacies types, which have been coded, thoroughly characterized in Tables 1 and 2, and assigned to subenvironments and environments with interpretation of bedforms and depositional processes. The most distinctive lithofacies, with particular emphasis on tuffs and accompanying volcaniclastic sandstones and conglomerates, are illustrated in Figures 3 and 4.

The tuffic horizons that are the subject of this study have been identified in most of the borehole sections examined, which points to their regional character (Figs. 1 and 2). So far, two new tuffs within sequence 2 and one within sequence 3 have been investigated. For unambiguous identification, they are marked with symbols consisting of a sequence number and an assigned Roman numeral, and characterized in detail in Table 3. Information on the regional distribution of the tuffs is included there as well. Two tuffic horizons (2.I, 2.II) have been identified in sequence 2 in the SE region , while one of them has been found in the NE region (2.I) and in the central region (2.II). The tuffic horizon (3.I) in sequence 3 has so far been investigated in the sections from the NE and central regions. Identification of further tuffic horizons is planned in the least explored SW area, and in sequence 3 in the NW and SE regions, where they are also most likely to occur, as indicated by the reconnaissance analysis of archived descriptions of borehole cores. However, confirmation of this thesis requires further sedimentological and petrographic-mineralogical studies.

Fining-upwards, non-gradational and coarsening-upwards cyclothems have been identified in the sections studied using the classification of Waksmundzka (2010, 2012, 2013). Fining-upwards cyclothems (Fig. 5) are composed of two members, the lower coarse-grained and the upper fine-grained. These are type IIa cyclothems (cf. e.g., Waksmundzka, 2012; Waksmundzka et al., 2021). Within the lower member, high-energy sandstone lithofacies are the most common: Sm (Fig. 4A), Sh2 and Sl; less frequent are low-energy facies: Sr, Sf (Fig. 4F) and Sx. High-energy conglomeratic lithofacies, Gm (Fig. 4B, D) and GSm, are encountered at the bases of some cyclothems. The upper members are most commonly represented by lithofacies Fm or Fh deposited from suspension, locally overlain by phytogenic lithofacies, i.e. mudstone and claystone *Stigmaria* soil R, and coals and carbonaceous claystones C. In the upper members, tuff lithofacies T locally occurs individually or in co-occurrence with lithofacies Fm and/or Fh. This is a peculiar feature of the fining-upwards cyclothems, previously undescribed. Among type IIa cyclothems, there is a lithofacies succession with the participation of tuffs: Sm Fm+T C, Sm Fm T, Sm T, Sh2 T, or without them: Gm Fm+Fh R C, SGm Sm Fm C, Sm Fm+Fh, Sr Sx Fn, Sf Fh.

The second type of fining-upwards cyclothem – IIb with successive FSh Fm, composed of low-energy lithofacies, is rare. Its thickness is ~3 m.The present-day thickness of type IIa fining-upwards cyclothems is 0.4–7.3 m. This comprises a smaller thickness of the lower member, typically reaching 0.2–2.8 m (maximum 4.2 m), and a relatively larger thickness of the upper member of 0.2–5.3 m, typically >4.4 m.

Non-gradational cyclothems (Fig. 5), in which no grain size gradation is present, are relatively numerous in the sections studied. They are categorized into a separate, previously uncoded type IIIb. This consists of lithofacies Fm (Fig. 4G) or Fh deposited from suspension, locally overlain by phytogenic lithofacies, i.e. mudstone and claystone *Stigmaria* soil R (Fig. 4E), and/or coals (Fig. 4C) and carbonaceous claystones C. Also, tuff lithofacies T may occur within this type of cyclothem. Type IIIb cyclothems are characterized by the lithofacies successions Fm R C, Fm C, Fm T C, Fh+T+Fm C, and their present-day thickness is 2.0–14.3 m.

Apart from those characterized above, there are also type Ic coarsening-upwards cyclothems (Fig. 6) in the sections studied (cf. Waksmundzka, 2013; Kozłowska and Waksmundzka, 2020), in which the upwards increase in grain size is manifested by the transition of claystone lithofacies Fm1 (Fig. 4K) and Fh1 into mudstones Fn (Fig. 4H), sandy mudstones FSh, and then into fine- and medium-grained sandstones Sh1, Sm or Sd. At the base of some coarsening-upwards cyclothems, carbonate lithofacies – limestones L and/or marls M – can occur, while phytogenic lithofacies of coals C are found at the top. Type Ic cyclothems are characterized by the most complete lithofacies

Table 1

Characteristics of the lithofacies occurred within fining-upwards and non-gradational cyclothems, and interpretation of their depositional environments

Lithofacies	Structure	Colour	Flora	Process	Pyroclastic volcanic eruption	Hyperconcentrated flow	Braided river	Anastomosing fluvial system	Fluvial floodplain
T Tuff	massive, horizontal lamination	creamy-dark red-yellow, yellow-dark red, yellow-black, creamy-yellow, grey-dark red, light grey-dark red, grey-red, dark red, creamy, yellow, brown, green	lack/plant chaff	fall of pyroclastic material and deposition on the ground surface	■				■
C Coal/carbonaceous claystone	massive	black	very common unlabeled	deposition of plant remains in peat swamp, coalification					■
R *Stigmaria* claystone/mudstone	nodular	light grey, dark grey, grey, black	*Stigmaria*, appendixes plant chaff	lack of flow deposition of clayey and silty suspension deposition of plant remains, pedogenic					■
Fm Massive claystone and mudstone	massive	light grey, grey, dark grey, dark grey-yellow, grey-green, grey-red, green, green-red, beige, bronze	plant chaff/lack	standing water – deposition of clayey and silty suspension					■
Fh Horizontal laminated claystone and mudstone	horizontal lamination	grey, dark grey, grey-yellow, grey-red							■
Fn Lenticular laminated siltstone	Lenticular lamination	dark grey, grey		rhythmic bed load transport in ripples (lower part of lower flow regime) and lack of flow – deposition from muddy and silty suspension					■
SFh Horizontal laminated sandy siltstone	Horizontal stratification	grey		deposition in upper plane bed (upper flow regime)				■	
Sf Flaser laminated sandstone	flaser lamination	beige, beige-dark grey, light grey, grey, grey-bronze, grey-red, grey-beige-red		rhythmic bed load transport in ripples (lower part of lower flow regime) and lack of flow – deposition from muddy and silty suspension			■	■	
Sr Ripple cross-stratified sandstone	ripple cross-lamination			rhythmic bed load transport in ripples (lower part of lower flow regime)			■		
Sx Large-scale cross-stratified sandstone	cross-stratification		plant chaff, carbonaceous matter	bedload transport in transverse bars or megaripples (lower or upper part of lower flow regime)			■		
Sh2 Horizontal stratified sandstone	horizontal stratification			deposition in upper plane bed (upper flow regime)		■	■	■	
Sl Low-angle cross-stratified sandstone	low-angle cross-stratification			bedload transport in transition from lower to upper flow regime			■		
Sm Massive sandstone	massive			hyperconcentrated flow		■	■		
SGm Massive gravelly sandstone						■			
GSm Massive sandy conglomerate	massive	light grey, grey, grey-cream, grey-beige, grey-bronze, grey-beige-pink, grey-green-bronze, bronze	lack	diffuse gravel sheet or longitudinal bar, transition from lower to upper flow regime			■	■	
Gm Massive conglomerate							■		

development. Their current thickness is 2.2–23 m. Type IIc coarsening-upwards cyclothems, of incomplete lithofacies development, lacking claystone or sandstone lithofacies, can occur in the study area too. The present-day thickness of type IIc cyclothems ranges from 2.2 to 22.0 m. The most abundant cyclothems in the boreholes are type IIIc non-gradational ones, which consist, from base to top, of limestone lithofacies L (Fig. 4L), and rarely marls M and claystones Fm1. A specific feature of type IIIc cyclothems, previously undescribed, is the occurrence of tuff lithofacies T within them, which can occur as interbeds within carbonate lithofacies – limestones L or marls M, or within claystone lithofacies Fm1 and Fh1. There is also a rare variety of type IIIc cyclothem, composed of limestones L, directly overlain by *Stigmaria* soil R (cf. Waksmundzka et al., 2021).

It was found that type Ic coarsening-upwards and type IIIc non-gradational cyclothems commonly include bioturbated claystone lithofacies Fd (Fig. 4I) and sandy mudstones FSd (Fig. 4J). These lithofacies types are observed in the bottom portions of the cyclothems and co-occur with claystone Fm1

Table 2

Characteristics of the lithofacies occurred within coarsening-upwards and non-gradational cyclothems and interpretation of their depositional environments

Lithofacies	Structure	Colour	Flora	Fauna	Process	Pyroclastic volcanic eruption	Shallow clay shelf	Shallow carbonate shelf	Shallow-water delta			
									Prodelta	Delta front	Mouth bar	Delta plain
T Tuff	massive, horizontal lamination	dark grey, grey-dark red, grey-cream, grey-green green-grey, yellow-grey, brown, light brown-green, creamy-dark red-yellow, creamy-dark red, creamy yellow, dark red-variegated, grey-red-variegated, creamy	lack/plant chaff	marine/lack	fall of pyroclastic material and deposition on the ground surface	■	■	■	■			■
C Coal/carbonaceous claystone	massive	black	very common unlabeled	lack	deposition of plant remains within peat swamp, coalification							■
R *Stigmaria* claystone/mudstone	nodular	grey, dark grey, black	*Stigmaria*, apendixes plant chaff		lack of flow, deposition of clayey or muddy suspension deposition of plant remains pedogenic							■
Sd Disturbed sandstone	disturbed	grey-brown	plant chaff/lack		disordering related to organic matter						■	
Sm Massive sandstone	massive	dark brown			deposition in upper plane bed (upper flow regime)						■	■
Sf Flaser laminated sandstone	flaser lamination	light grey, creamy			rhythmic bedload transport in ripples (lower part of lower flow regime) and lack of flow – deposition from muddy and silty suspension						■	
Sh1 Horizontal laminated sandstone	horizontal lamination				deposition in lower plane bed from sandy suspension						■	
FSh Horizontal laminated sandy siltstone		dark grey			deposition in lower plane bed from silty and sandy suspension					■		
FSd Disturbed sandy siltstone	disturbed	dark grey, grey, creamy			bioturbation by benthic organisms				■	■		
Fd Disturbed mudstone/siltstone		dark grey, grey							■	■		
Fn Lenticular laminated siltstone	lenticular lamination	grey			rhythmic bedload transport in current and wave ripples and lack of flow – deposition from muddy and silty suspension					■		
Fh2 Horizontal laminated mudstone	horizontal lamination	creamy, grey-red-cream			lack of flow – deposition from clayey and muddy suspension				■	■		
Fh1 Horizontal laminated claystone		grey, dark grey, black	lack	marine	lack of flow – deposition from clayey suspension		■		■			
Fm2 Grey massive claystone	massive	light grey, grey	plant chaff	lack/ fresh-water								■
Fm1 Black massive claystone		dark grey, black	lack	marine/ lack			■		■			
M Marl		black, dark grey		marine	lack of flow – deposition from clayey suspension deposition of calcareous marine faunal remains			■				
L Limestone	massive, nodular	grey, dark grey, filemot, greige, beige			deposition of limy marine faunal remains			■				

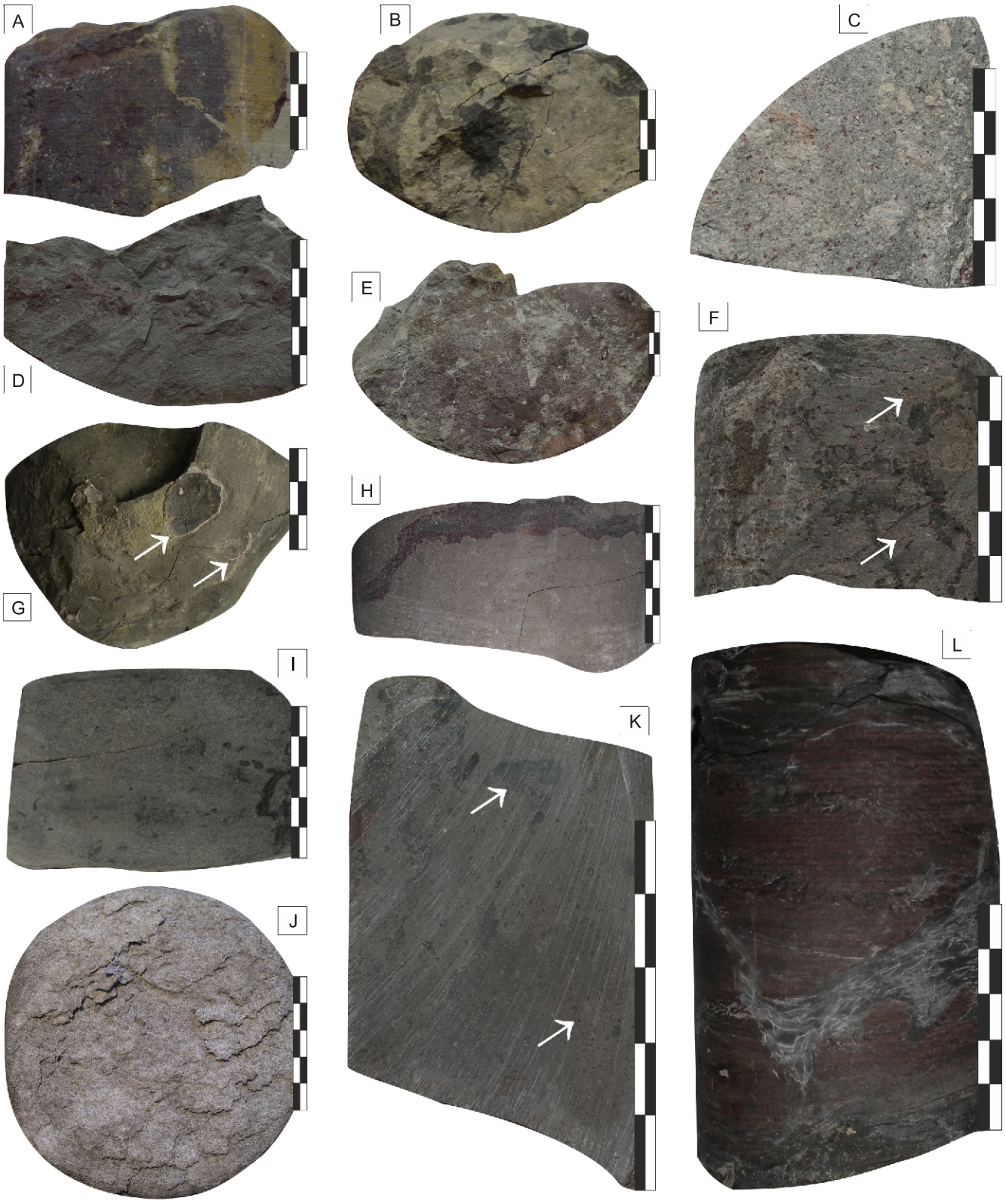

Fig. 3. Examples of tuff lithofacies; correlation horizons: 2.I – A, B, D, G, I; 2.II – Figs J, K; 3.I – C, E, F, H, L; fine-ash tuffs – A, B, D-L; coarse-ash tuff – C

A – Łuków IG 5 borehole; depth 1206.75 m; **B** – Korczmin IG 1 borehole; depth 1333.0 m; **C** – Radzyń IG 1 borehole; depth 927.7 m; **D** – Marynin 1 borehole; depth 1354.2 m; **E** – Radzyń IG 1 borehole; depth 925.4 m; **F** – Glinnik 2 borehole; depth 2257.37 m; numerous siderite spherulites (arrows); **G** – Terebin IG 1 borehole; depth 1337.8 m; brachiopod shells (arrows); **H** – Łuków IG 4 borehole; depth 1539.95 m ; **I** – Korczmin IG 1 borehole; depth 1337.8 m; **J** – Terebin IG 1 borehole; depth 1273.77 m; **K** – Nasutów 1 borehole; depth 2186.2 m; bubbly texture arrowed); **L** – Nasutów 2 borehole; depth 2295.45 m; units on scale bar = 1 cm

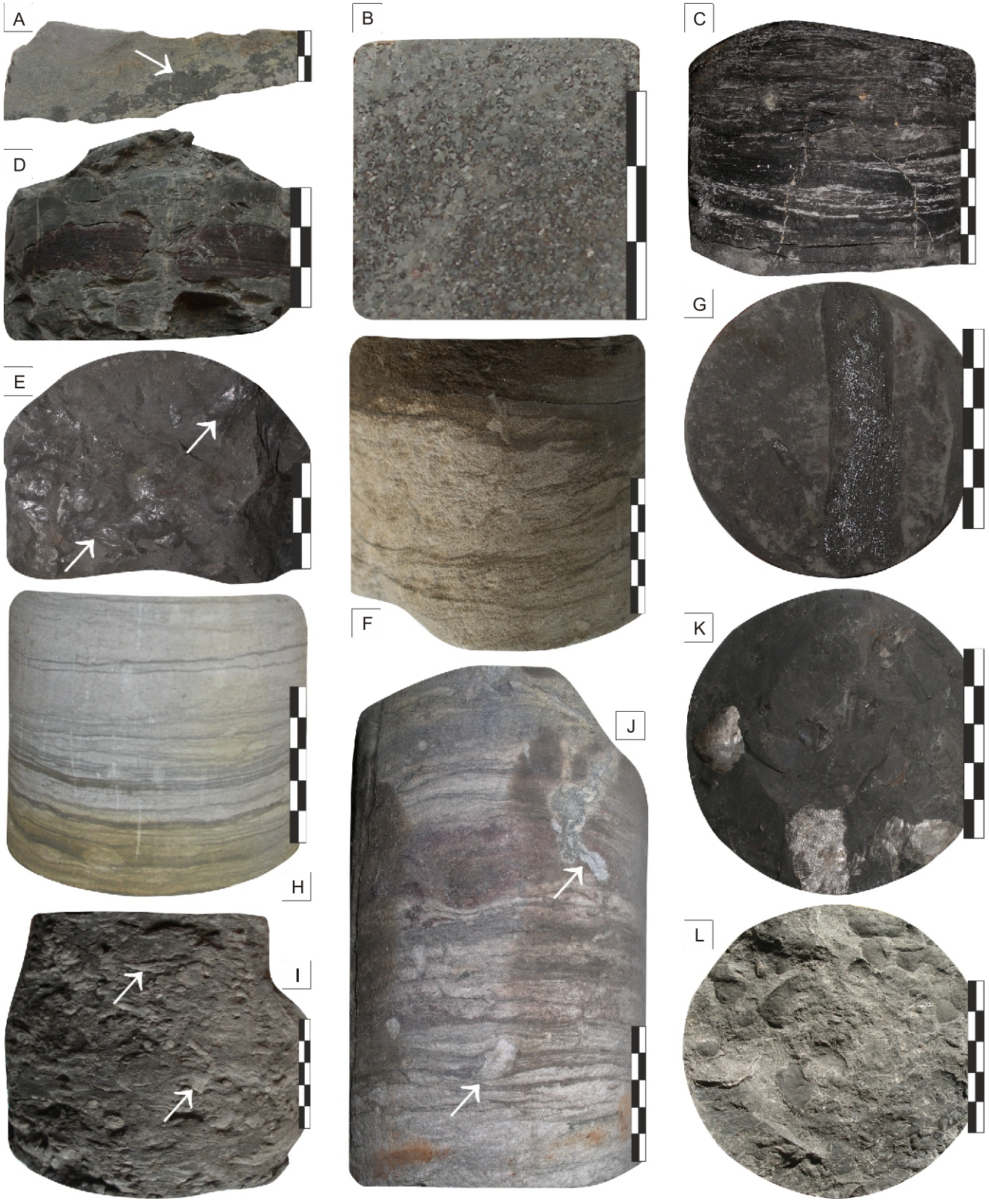

Fig. 4. Examples of the most distinctive lithofacies

A – Lithofacies Sm: fine-grained massive sandstone; in places there is a concentration of tuff material (arrow); Korczmin IG 3 borehole; depth 1350.70 m; LST of sequence 2; **B** – Lithofacies SGm: massive gravelly sandstone; Nasutów 1 borehole; depth 2162.35 m; LST of sequence 3; **C** – Lithofacies C: coal; Łuków IG 4 borehole; depth 1538.01 m; TST of sequence 3; **D** – Lithofacies Gm: massive conglomerate; Łuków IG 4 borehole; depth 1546.7 m; LST of sequence 2; **E** – Lithofacies R: clayey *Stigmaria* soil; slickensides-related compaction (arrowed); Łuków IG 4 borehole; depth 1538.8 m; TST of sequence 3; **F** – Lithofacies Sf: fine-grained flaser-laminated sandstone; lamination highlighted with brown tuff material; Marynin 1 borehole; depth 1359.32 m; LST of sequence 2; **G** – Lithofacies Fh: horizontal laminated mudstone with coalified fragment of calamite; Nasutów 2 borehole; depth 2288.63 m; TST of sequence 3; **H** – Lithofacies FSh: horizontal laminated sandy siltstone; upwards it becomes lithofacies Sh: fine-grained horizontally laminated sandstone; Łuków IG 5 borehole; depth 1195.11 m; HST of sequence 3; **I** – Lithofacies Fd: disturbed mudstone with common bioturbation (arrows); Korczmin IG 1 borehole; depth 1332.3 m; correlation horizon 2.B; TST of sequence 2; **J** – Lithofacies FSd: disturbed sandy siltstone with common bioturbation; brown colour related to the concentration of tuff material (arrows); Marynin 1 borehole; depth 1350.55 m; correlation horizon 2.B; TST of sequence 2; **K** – Lithofacies Fm1: black massive claystone with brachiopods; Nasutów 2 borehole; depth 2284.64 m; TST of sequence 3; **L** – Lithofacies L: limestone with faunal detritus; Korczmin IG 3 borehole; depth 1316.3 m; TST of sequence 2; units on scale bar = 1 cm

Table 3

Characteristics of tuffic correlation horizons 2.I, 2.II, 3.I and bioturbated horizon 2.B

Chronostratigraphy	Sequence Stratigraphy		Correlation horizon	Thickness interval of horizon [m]	Lublin Basin			
	Number of sequence	Systems tract		Present/ Decompacted	NE	SW	CENTRAL	SE
Upper Visean	3	TST	3.I	1.0–8.0/ ~5–40	+	?	+	?
	2	HST	2.II	0.2-6.0/ ~1–30	–	?	+	+
		TST	2.B	0.3–1.2/ ~1.4–5.5	–	?	–	+
		TST	2.I	0.4–4.8/ ~2–22	+	?	–	+

+ presence; ? not recognized; – absence

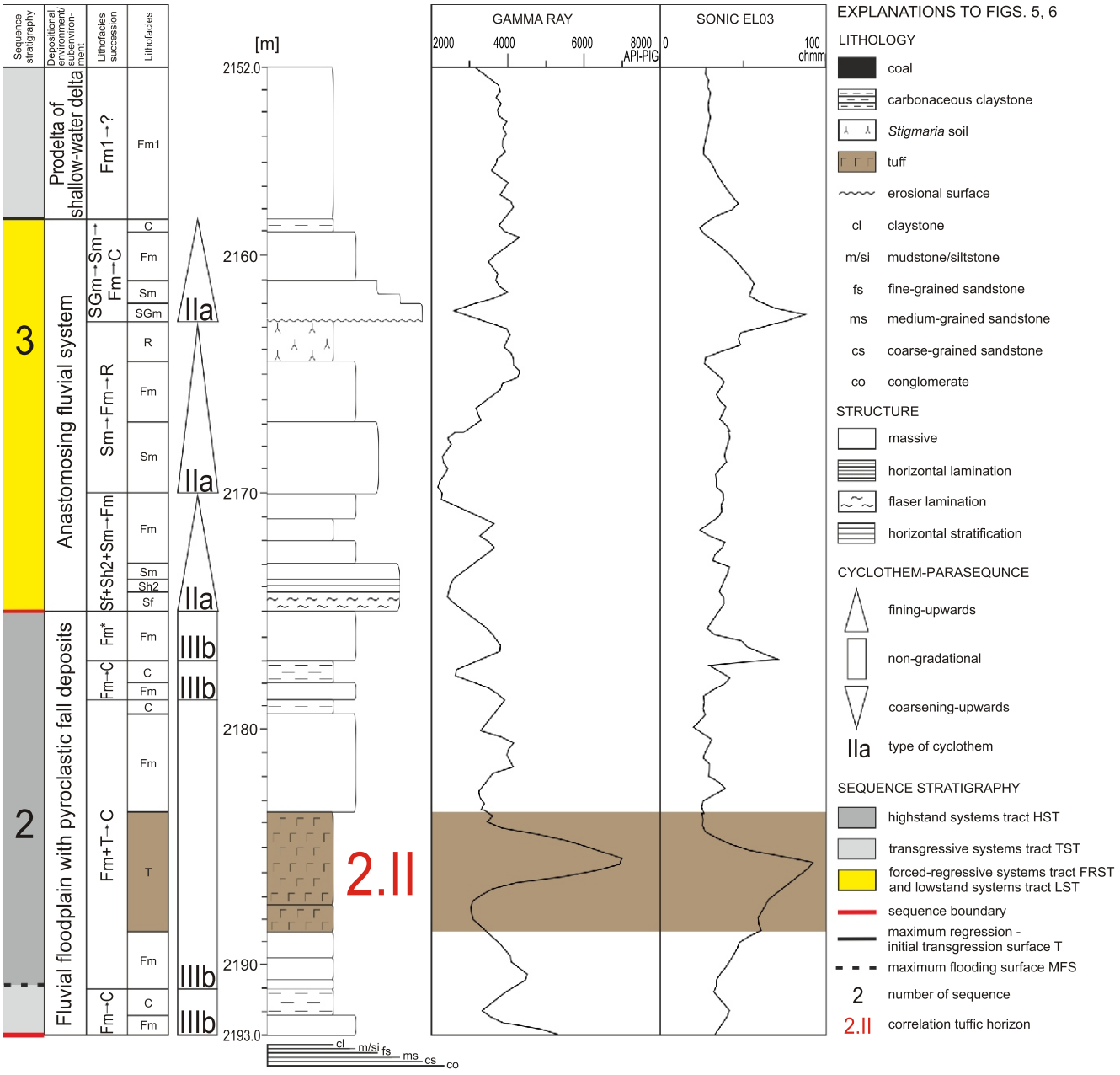

Fig. 5. Example lithofacies, fining-upwards and non-gradational cyclothems (parasequences) deposited in anastomosing fluvial system and fluvial floodplain environments with a pyroclastic episode of tuffic horizon 2.II, Nasutów 1 borehole

* – erosional top of the lithofacies succession

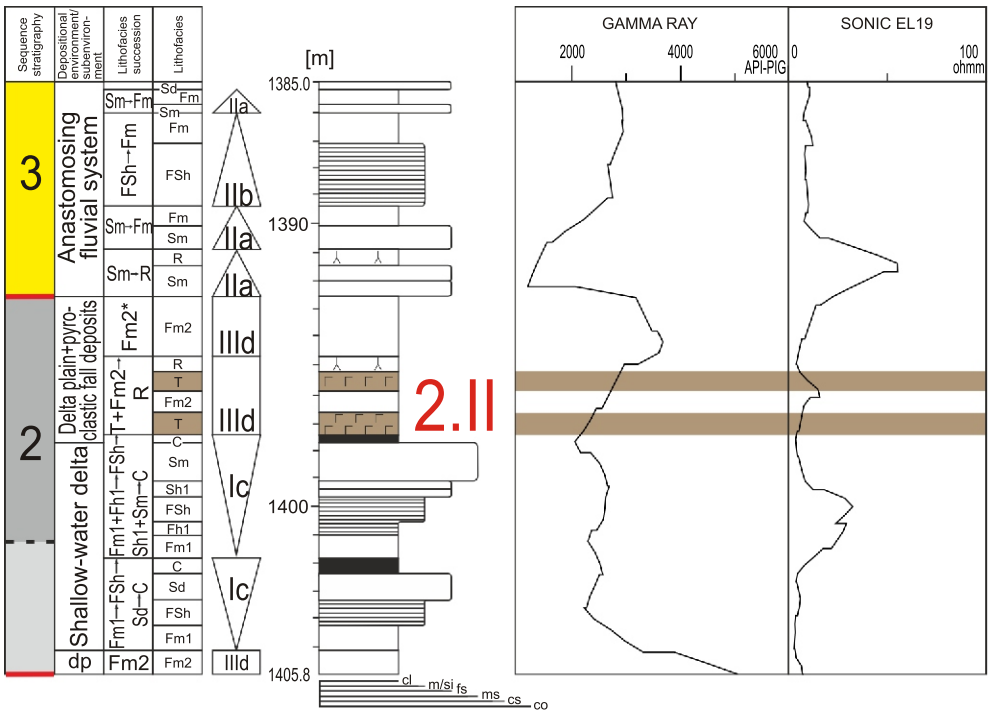

Fig. 6. Example lithofacies, coarsening-upwards and non-gradational cyclothems (parasequences) deposited in a shallow-water delta environment with a pyroclastic episode, Świdnik 22 borehole

dp – delta plain; * – erosional top of the lithofacies succession

and mudstone Fm3 lithofacies. Due to the widespread occurrence of these bioturbated lithofacies, just above the 2.I tuff horizon within sequence 2 in the SE area, they too have been considered as a correlative horizon, and labelled 2.B. The present-day thickness of this horizon is 0.3–1.2 m (Table 3).

TUFF LITHOFACIES

Three horizons of regional significance (Table 3), in which the tuff T lithofacies (Fig. 3) occurs, have been identified within deposits of sequences 2 and 3: (1) fine-ash tuffs, (2) coarse-ash tuffs, and (3) one tuffic horizon with a fining-upwards trend and transition from coarse-ash to fine-ash tuff. They are characterized by massive structures and may rarely be horizontally laminated (Tables 1 and 2).

In the basal parts of sequence 2, there is the lower tuffic horizon, marked 2.I. It has been identified in cored sections of boreholes drilled in the NE (Fig. 7) and SE (Fig. 9) regions, and is represented by two types. The first type is characterized by diverse, distinct, variegated colours: creamy-dark red-yellow, yellow-dark red, yellow-black, creamy-yellow, grey-dark red, light grey-dark red, dark red, creamy, yellow, and brown, as well as by the presence of irregular aggregations of pyrite or siderite. This type is encountered, for example, in the Łuków IG 4 and Łuków IG 5 boreholes (Fig. 3A) in the NE, and in the Korczmin IG 1 (Fig. 3B, I) and Korczmin IG 3 boreholes in the SE. The present-day thickness of tuff 2.I is 0.4-4.8 m, and after decompaction it is ~2-22 m.

The other type of tuff, 2.I, with a present thickness of 0.5 m (decompacted thickness about 2.5 m), occurring in the SE in the Marynin 1 (Fig. 3D), Terebin IG 1 (Fig. 3G) and Terebin IG 3 boreholes, is characterized by a uniform dark grey or green-grey colour and the presence of bioclasts: single brachiopod shells or fish scales.

The second, upper tuffic horizon, marked 2.II, which occurs in the upper part of sequence 2 in the boreholes located in the central (Fig. 8) and SE (Fig. 9) regions, is also represented by two types. The first type is found in the central region, e.g. in the Nasutów 1 (Fig. 3K), Nasutów 2, Glinnik 2 and Świdnik 22 boreholes, and is less varied in colour (creamy, brown, green, grey-green or grey-red). Relatively common coalified plant detritus or larger fragments of calamites, and in places scattered siderite or siderite spherulites, are found in this type. Its present-day thickness is 0.8–6 m and a decompacted thickness is ~4–30 m. This horizon can be identified also on well logs (gamma ray, sonic EL03) in the form of characteristic maxima, especially when it is thick, e.g. in the Nasutów 1 borehole (Fig. 5). However, where it is less thick or consists of two thin layers separated by lithofacies Fm2 (Świdnik 22 borehole; Fig. 6), it cannot be clearly identified on well logs.

The other type of tuffic horizon, 2.II, has been identified in the upper part of sequence 2, in the Korczmin IG 1, Korczmin IG 3, Terebin IG 1 (Fig. 3J) and Terebin IG 3 boreholes from the SE region (Fig. 9). Its position is remarkable as it occurs as an interbed within a thick (several metres) layer of grey or dark grey organodetrital limestone and marl, containing marine echinoderm, brachiopod, foraminifer and coral remains. The lithological characteristics and colour of tuff 2.II, which can be green-grey, yellow-grey, brown or light brown-green, distinguish it clearly from the underlying and overlying carbonates. Infrequent brachiopod shells, coalified plant detritus and pyrite impregnations are locally present within the tuff. Its present-day thickness is 0.2–2.5 m and a decompacted thickness is ~1.0–11.5 m.

Another tuffic horizon located in the lower part of sequence 3 is marked with the symbol 3.I. So far, it has been found in the Łuków IG 4, Łuków IG 5, Radzyń IG 1 and Siedliska IG 1 boreholes from the NE region (Fig. 7), and in the Nasutów 2 and

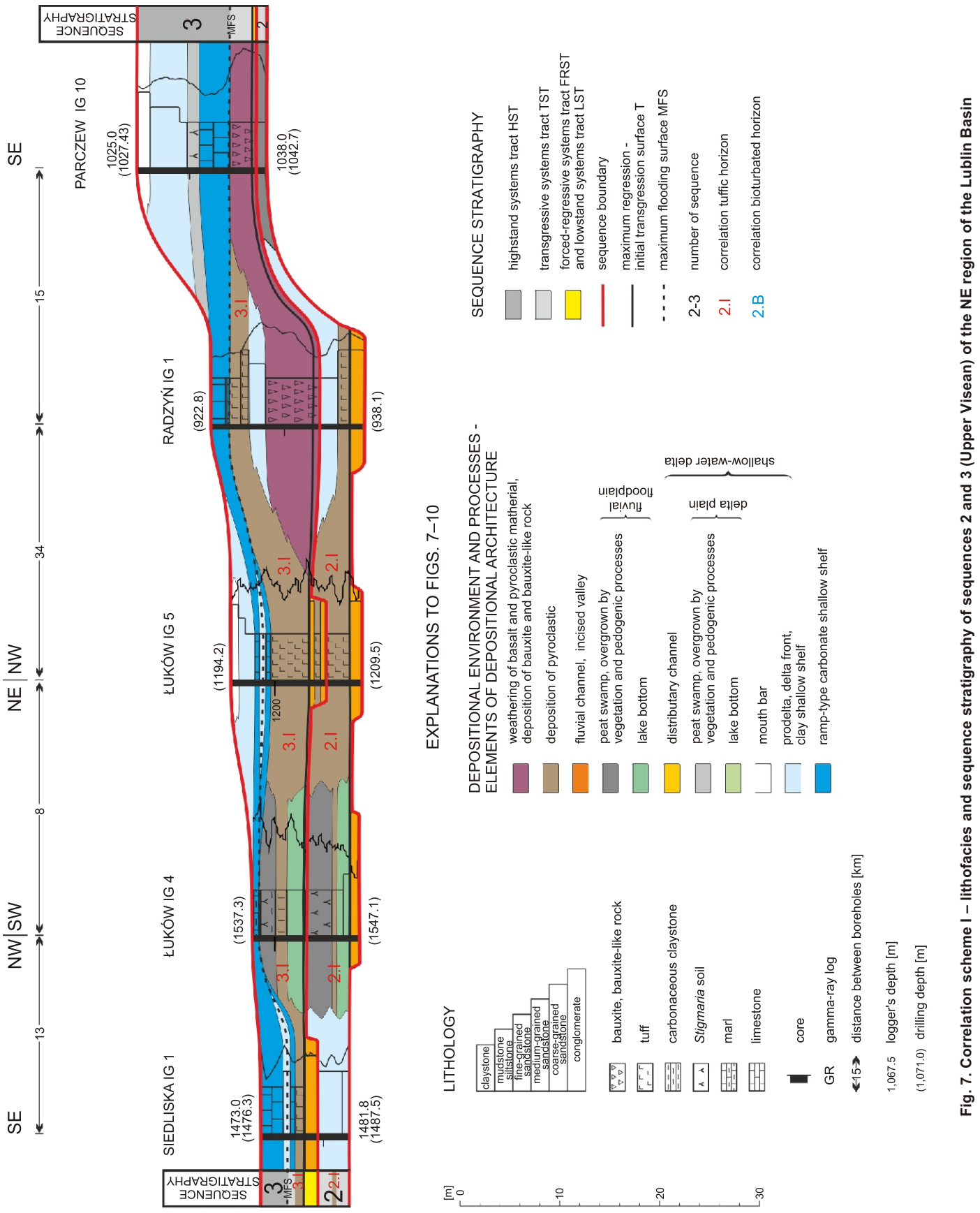

Fig. 7. Correlation scheme I – lithofacies and sequence stratigraphy of sequences 2 and 3 (Upper Visean) of the NE region of the Lublin Basin

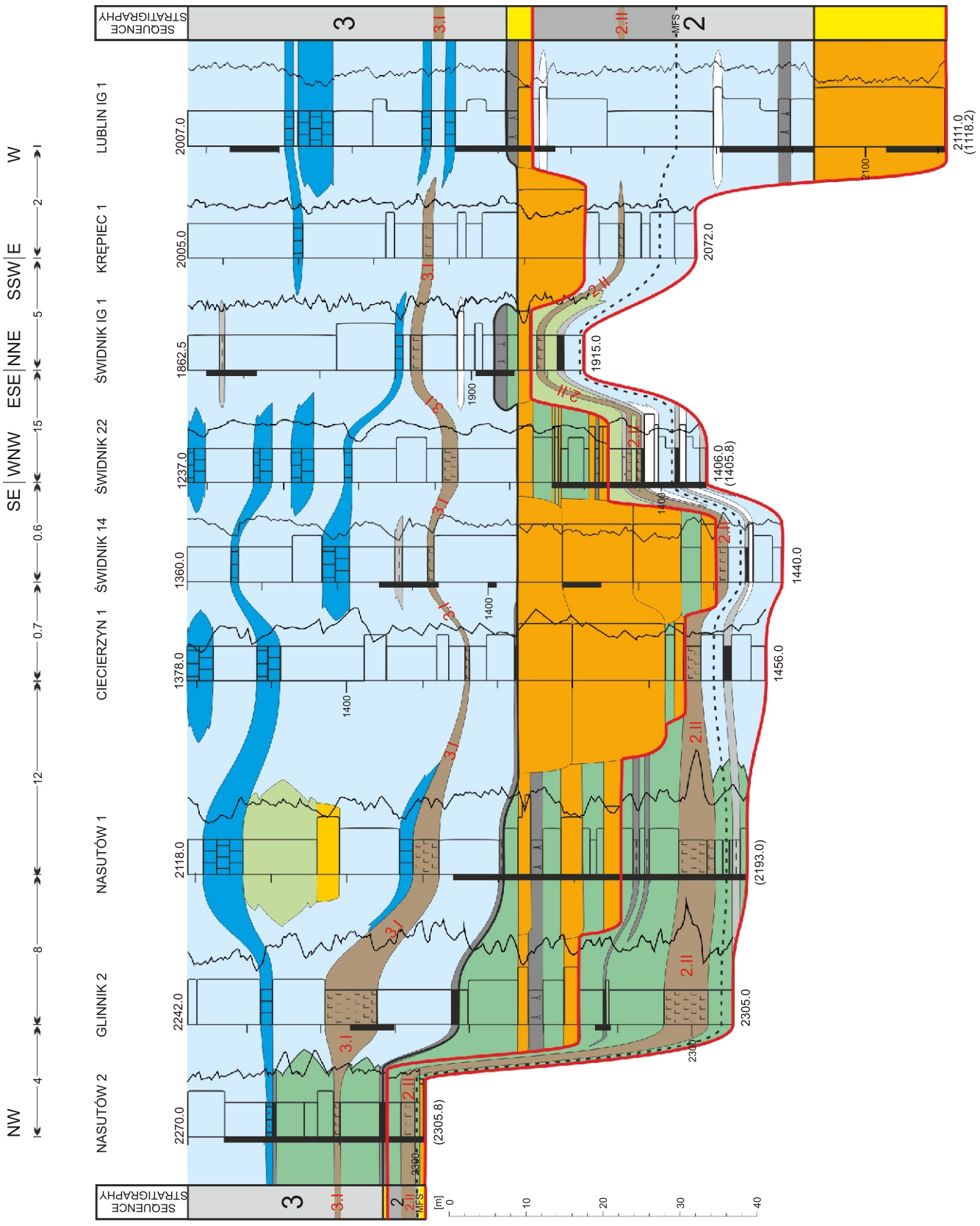

Fig. 8. Correlation scheme II – lithofacies and sequence stratigraphy of sequences 2 and 3 (Upper Visean) of the central region of the Lublin Basin

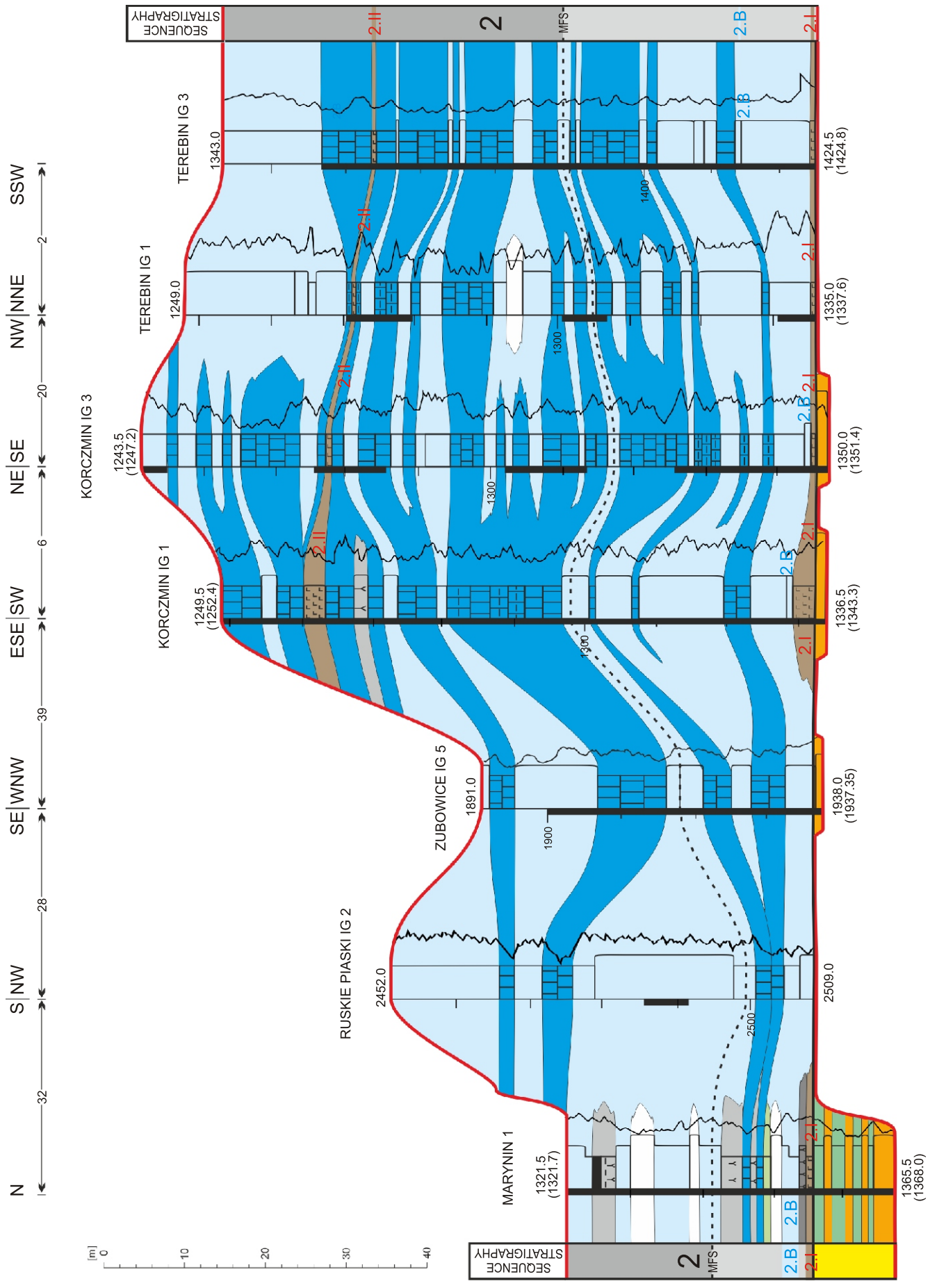

Fig. 9. Correlation scheme III – lithofacies and sequence stratigraphy of sequence 2 (Upper Visean) of the SE region of the Lublin Basin

Glinnik 2 boreholes from the central region (Fig. 8). In the remaining sections investigated, its presumed presence is interpreted on gamma ray and electrical resistivity curves at the site of clear maxima.

In the NE region, tuff 3.I occurs in a peculiar position, directly beneath a several-metres-thick layer of organodetrital and, in places, nodular limestones, which is the only one in sequence 3 (Fig. 7). The tuff is characterized by creamy-dark red-yellow, creamy-dark red, creamy yellow, dark red-variegated, grey-red-variegated or creamy colours (Fig. 3C, E, H). It contains a small amount of brachiopod and bivalve shell material, coalified plant detritus, and scattered hematite. Calcification of the tuff (reaction with HCl) is its characteristic feature. In the Radzyń IG 1 borehole, a fining-upwards trend is observed within this tuff. The thickness of the tuff is ~1–5 m (decompacted ~5.6–23 m).

In the central region, tuffic horizon 3.I occurs in the lower part of sequence 3, several metres below the first limestone layer in the sequence (or in one case directly below it; Fig. 8). The tuff and limestone are separated by homogeneous claystones and/or mudstones. Tuff 3.I is characterized by a grey-dark red, grey-cream or grey-green colour, the presence of sparse coalified plant detritus, scattered hematite, and siderite spherulites (Fig. 3F, L). The thickness of horizon 3.I is 1-8 m (decompacted ~5–40 m).

DEPOSITIONAL ENVIRONMENTS AND SEQUENCE STRATIGRAPHY

The lithological and facies characteristics, along with elements of sequence stratigraphy of sequences 2 and 3 in the NE and central regions, are shown in Figures 7 and 8, and of sequence 2 in the SE region in Figure 9.

SEQUENCE 2

Sequence 2 is found across most of the Lublin Basin area, except in the NW region (Waksmundzka, 2010). Its present thickness is extremely small (~1–5 m) in the NE (Fig. 7). The area was characterized by a low subsidence rate due to both the shallow occurrence of crystalline rocks of the East European Craton and the presence of thick basalt bodies in the immediate basement, belonging to sequence 1 of Tournaisian age (Waksmundzka et al., 2021). The relatively small thickness in the centre of the basin in the area of the Nasutów 2, Świdnik IG 1, Świdnik 14 and Świdnik 22 boreholes (Fig. 8) can presumably also be related to the presence of basaltic rocks in the immediate basement. The small thickness could result also from erosional reduction of near-top strata of sequence 2 during the next falling and RSL lowstand of sequence 3. The thickness of sequence 2 in the basin generally increases towards the S and SE. In the area of the Lublin IG 1 borehole, it reaches ~55 m, and the greatest thicknesses, attaining ~92 m, are recorded in the SE (Fig. 9), where the greatest subsidence rate took place (Kozłowska and Waksmundzka, 2021).

The lower boundary of sequence 2 is an erosional surface formed during the falling of RSL. It forms the base of the Visean deposits and runs below a bed of volcaniclastic sandstones and conglomerates deposited in shallow (~0.5–0.8 m), highly aggradational, high-energy river channels during a lowstand and a slow initial rise of RSL. This is indicated by the dominance of the high-energy lithofacies Sm, Sh2 and Sl. These are overlain by the thick upper members of type IIa fining-upwards cyclothems, composed of Fm and Fh lithofacies deposited on a fluvial floodplain. It should be assumed that these channels operated in an anastomosing system, and that their filling and waning were related to a RSL rise. Similar fluvial environments described by Kozłowska and Waksmundzka (2020) also existed in the Lublin Basin in the Serpukhovian and Bashkirian. Elsewhere in the world they are known from the Carboniferous in Canada (Rust, 1984; Nadon, 1994).

Only in the area of the Lublin IG 1 and Marynin 1 boreholes were large incised valleys formed, attaining depths of ~25 m and ~40 m, respectively. In the central region, the incised valley was filled mainly by high-energy volcaniclastic sandstones and conglomerates that formed as a result of hyperconcentrated flow (Waksmundzka, 2010; Waksmundzka et al., 2021). By contrast, the incised valley in the area of Marynin 1 borehole was filled by braided river sediments (Kozłowska and Waksmundzka, 2020).

In the NE and SE regions, the lower tuffic horizon 2.I, which reaches the greatest thickness in the Łuków IG 5 and Korczmin IG 1 boreholes, occurs at the top of LST deposits. Tuff lithofacies T overlies channel sandstones and conglomerates or co-occurs with lithofacies deposited on the floodplain. The pyroclastic deposits accumulated on the alluvial plain and the material was derived from volcanic cones active in these areas since at least the Late Tournaisian (Waksmundzka et al., 2021).

In part of the SE region, tuff 2.I was deposited on a fluvial floodplain, while in the vicinity of the Terebin IG 1 and Terebin IG 3 boreholes, in a marine environment, in prodelta or shallow clay-dominated shelf settings, as indicated by the presence of brachiopods and fish scales within the tuff. A marine reservoir existed in this area already at the time of the RSL lowstand and probably encompassed also the area of the Ruskie Piaski IG 2 and Zubowice IG 5 boreholes, located farther to the SW. The presence of the sea in this area can be associated with a high subsidence rate and the formation of large accommodation space in the Late Visean, as indicated by the existence of a depocentre previously already interpreted to occur here (Waksmundzka, 2010).

The initial transgression surface, which is defined by the base of deltaic and marine deposits, runs above tuffic horizon 2.I. The deposits are represented mainly by claystone and mudstone lithofacies Fm1, Fm3 and Fh1, deposited on a shallow clay-dominated shelf and in prodelta settings of a shallow-water delta, as well as by the interbedded lithofacies of limestones L and marls M that accumulated on a shallow carbonate shelf (Flügel, 2004). These deposits form the TST and HST that compose the upper part of sequence 2. The most common cyclothems among these deposits are type IIIc non-gradational ones, indicating the dominance of aggradation. Complete type Ic coarsening-upwards cyclothems are rare. The cyclothems amid sedimentary aggradation and progradation. A MFS has been identified within the shallow shelf claystones. In the NE region, only thin (a few metres) TST deposits are present, and the HST is absent due to erosion and/or nondeposition during the subsequent RSL fall. The characteristics of these environments from the Lublin Basin, together with the description of cyclicity, were previously described by Skompski (1988, 1995a, b) and Waksmundzka (1998, 2010, 2013).

In most of the sections from the SE region (Fig. 9), bioturbated lithofacies (Fig. 4I, J) are encountered directly above tuff 2.I, which are marked in the correlative horizon 2.B. This occurs immediately above the initial transgression surface, within the prodelta or shallow clay shelf deposits, and, like this surface, may be considered an isochronous correlative horizon. The strong bioturbation of the bottom sedimentary layer indicates in-

creased activity of benthic organisms, presumably triggered by nutrient abundance. Possibly, after volcanic eruption, organic debris along with pyroclastic material entered the sea, providing a rich food source for benthos (Carrillo and Diaz-Villanueva, 2021).

The second, upper tuffic horizon 2.II occurs in the upper part of sequence 2 that comprises the HST. Its position in the sections from the central region is peculiar, as it occurs only a few metres above the MFS, i.e. at the base of HST deposits. In the sections located farther to the NW (Nasutów 1, Fig. 5; Nasutów 2; Glinnik 2 boreholes), it was deposited on a fluvial floodplain, and farther to the SE, in the prodelta and shallow clay shelf environments and, in places, on a delta plain (Świdnik IG 1, Świdnik 22 boreholes). In the SE region, tuffic horizon 2.II occurs in the upper part of the HST as a characteristic interlayer within a limestone and marl bed. After volcanic eruption, pyroclastic material formed a thick layer, in places reaching up to ~12 m (decompacted thickness in the Korczmin IG 1 borehole), on a carbonate ramp, which probably caused a temporary extirpation of organisms living there (cf. Simon et al., 2017). However, the ecosystem recovered, as shown by the return of sedimentation of carbonate organic remains, also above tuff 2.II, which are components of the overlying carbonate bed. Diagenetic altered volcanic ashes are quite often found in Mississippian carbonate deposits, such as in the Namur-Dinant Basin in Belgium (cf. Pointon et al., 2018).

SEQUENCE 3

Sequence 3 is present throughout the Lublin Basin (Waksmundzka, 2010). It has an extremely small thickness in the NE (Fig. 7), ranging from 4 to 10 m, and, like the thickness of sequence 2, increases towards the S and SE. In the central part (Fig. 8) its thickness is 80–110 m, and a maximum value of ~180 m is found in the SE region. The thickness variation is probably related to a greater rate of basement subsidence in the centre of the basin and in the SE region, as well as to the formation of large accommodation space. The thickness of sequence 3 has been reduced to some extent at the top during the subsequent falling and lowstand of RSL of sequence 4.

The lower boundary of sequence 3, coinciding with the upper boundary of sequence 2, is an erosional surface that formed during the RSL fall. Above the surface, there are fluvial deposits representing the LST. In the central region, the sequence boundary is placed below a volcaniclastic sandstone bed that occurs at the base of an incised valley. This valley seems to have stretched from the area of the Glinnik 2 borehole, through the region of the Nasutów 1, Ciecierzyn 1 and Świdnik 14 boreholes, to the vicinity of Świdnik 22. Its greatest depth of ~34 m is found in the Ciecierzyn 1 and Świdnik 14 boreholes. It is filled almost exclusively with sandstones. The sparse core material does not provide a basis for reconstruction of the fluvial environments that existed in this area. One can only suppose, based on the presence of sandstone lithofacies Sm in the 5-m-long core section of the Świdnik 14 borehole, that sedimentation took place from high-energy, highly aggradational hyperconcentrated flow (cf. Martinsen, 1994; Svendsen et al., 2003). Analogous processes of incised valley filling in the area of the nearby Lublin IG 1 borehole had operated also earlier, during the formation of sequence 2. In the area of the Glinnik 2, Nasutów 1 and Świdnik 22 boreholes, the incised valley was filled with fluvial sediments, including both channel sandstone lithofacies and overbank claystone-mudstone and phytogenic lithofacies. The presence of type IIa fining-upwards cyclothems and the extreme thickness of floodplain deposits indicate an anastomosing channel system environment. Only in the northernmost part of the central region did no incised valleys form. Sedimentation took place exclusively on a fluvial floodplain, within peat swamps (lithofacies coals C).

In the NE region, the LST-forming deposits include sandstones of shallow-water (~0.8–1 m) braided channels (Siedliska IG 1, Łuków IG 5 boreholes), and a thin (0.1 m) coal layer that formed as peat bogs on a fluvial floodplain (Nasutów 2 borehole). Farther to the E, around the Radzyń IG 1 and Parczew IG 10 boreholes, bauxites were deposited during the lowstand of sequence 3 (Waksmundzka et al., 2021).

The initial transgression surface in the central region runs at the top of fluvial deposis or at the base of the coal and carbonaceous claystone C lithofacies, or within the bauxite bed (Waksmundzka et al., 2021). Above, there are TST deposits that formed during a RSL rise. In the central region, these are represented mainly by claystone and mudstone lithofacies deposited on a shallow clay shelf and the prodelta of a shallow-water delta. Less common are sandstones deposited in either mouth bars or deltaic distributary channels. Limestones and marls, locally reaching considerable thicknesses (~12 m), are found as interbeds and were deposited in a shallow carbonate shelf environment. As in sequence 2, most common are type IIIc non-gradational cyclothems, and less common are complete type Ic coarsening-upwards cyclothems. This deposition occurred with mainly during the aggradation and, to a lesser extent, the progradation of sediments. The MFS is interpreted to occur at the maximum excursion on gamma ray logs within claystones of the shallow clay shelf. Above it are HST deposits represented by facies very similar to those of the TST. In the NE region, the TST and HST deposits are very thin. These were deposited in similar environments to those developed in the central area: deltaic, shallow clay shelf, and carbonate shelf.

Tuffic horizon 3.I in the central region occurs within TST deposits – shallow-shelf and prodelta claystones and mudstones – except in the area of the Nasutów 2 borehole, where it is associated with fluvial floodplain deposits. The thickest layer of post-eruption volcanic pyroclastic material, at ~15–40 m (decompacted thickness), is found in the area of the Glinnik 2 and Nasutów 1 boreholes (Fig. 8). In these boreholes, tuff 2.II also attains its maximum thickness, indicating that the eruptive centre was located not far away, and presumably had been active in the area since at least the Late Tournaisian (Waksmundzka et al., 2021).

Tuff 3.I in the NE region (Fig. 7) was probably deposited on a fluvial floodplain (Siedliska IG 1, Łuków IG 4, Łuków IG 5 boreholes), and in the area of the Radzyń IG 1 borehole, in the prodelta of a shallow-water delta. The fining-upwards trend observed in the tuff created during deposition in the marine basin. Lithological and facies correlation indicates that tuff horizon 3.I corresponds to the bauxite bed found in sequence 3 in the Radzyń IG 1 and Parczew IG 10 boreholes, and that both may have a similar pyroclastic origin. This conclusion should be regarded as preliminary and needs confirmation by further studies. To date, no bauxite rocks have been found in the existing borehole cores, and their analysis has been so far based on archived data (Waksmundzka et al., 2021).

PETROGRAPHIC CHARACTERISTICS

The tuffs and volcaniclastic rocks (conglomerates, sandstones and mudstones) identified in sequences 2 and 3 are illustrated in Figures 10 and 11.

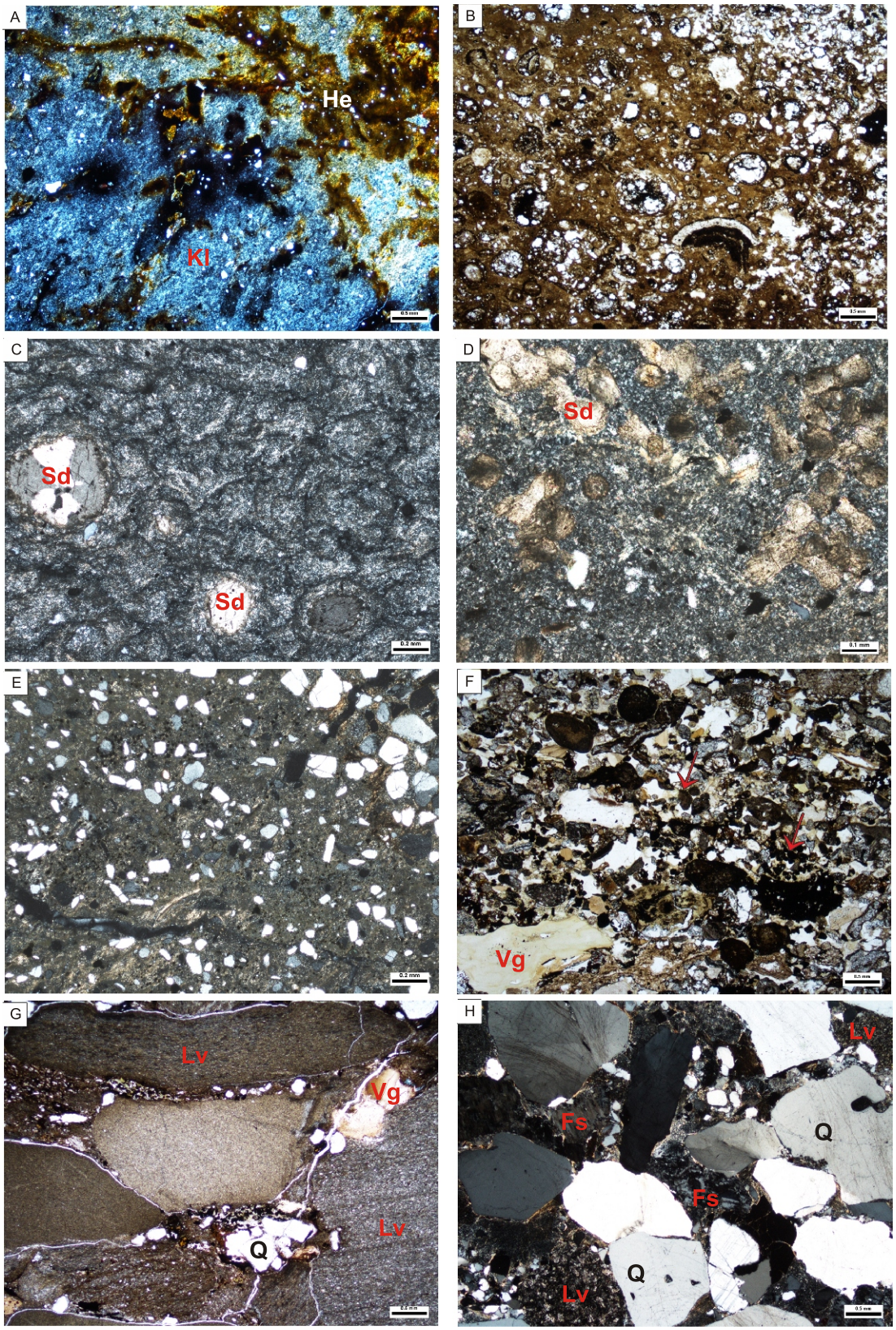

Fig. 10. Microphotographs taken by polarizing microscope

A – strongly altered fine-ash vitric tuff; volcanic glass altered to kaolinite (Kl); hematitization (He); Łuków IG 5 borehole; depth 1206.75 m; sequence 2; horizon 2.I; crossed polars; **B** – fine-ash vitric tuff with a bubbly texture; Nasutów 1 borehole; depth 2186.2 m; sequence 2; horizon 2.II; without analyser; **C** – fine-ash vitric tuff with a perlitic texture; volcanic glass altered to clay minerals; siderite (Sd); Glinnik 2 borehole; depth 2257.37 m; sequence 3; horizon 3.I; crossed polars; **D** – fine-ash vitric tuff; volcanic glass altered to clay minerals; numerous siderite (Sd); Marynin 1 borehole; depth 1354.2 m; sequence 2; horizon 2.I; crossed polars; **E** – fine-ash vitric-crystal tuff; quartz grains in part of volcanic origin; Korczmin IG 1 borehole; depth 1333.0 m; sequence 2; horizon 2.I; crossed polars; **F** – coarse-ash vitric-lithic tuff; volcanic glass fragments (Vg); abundant anatase (arrows); Radzyń IG 1 borehole; depth 927.7 m; sequence 3; horizon 3.I; without analyser; **G** – fine-grained volcaniclastic polymictic orthoconglomerate; volcanic rock fragments (Lv) mainly rhyolite bonded by sandy-clay matrix; Łuków IG 4 borehole; depth 1546.7 m; sequence 2; without analyser; **H** – very fine-grained volcaniclastic polymictic orthoconglomerate; volcanic rock fragments (Lv); feldspar (Fs), volcanic quartz (Q) bonded by sandy-clay matrix; Niedrzwica IG 1 borehole; depth 2190.0 m; sequence 2, crossed polars

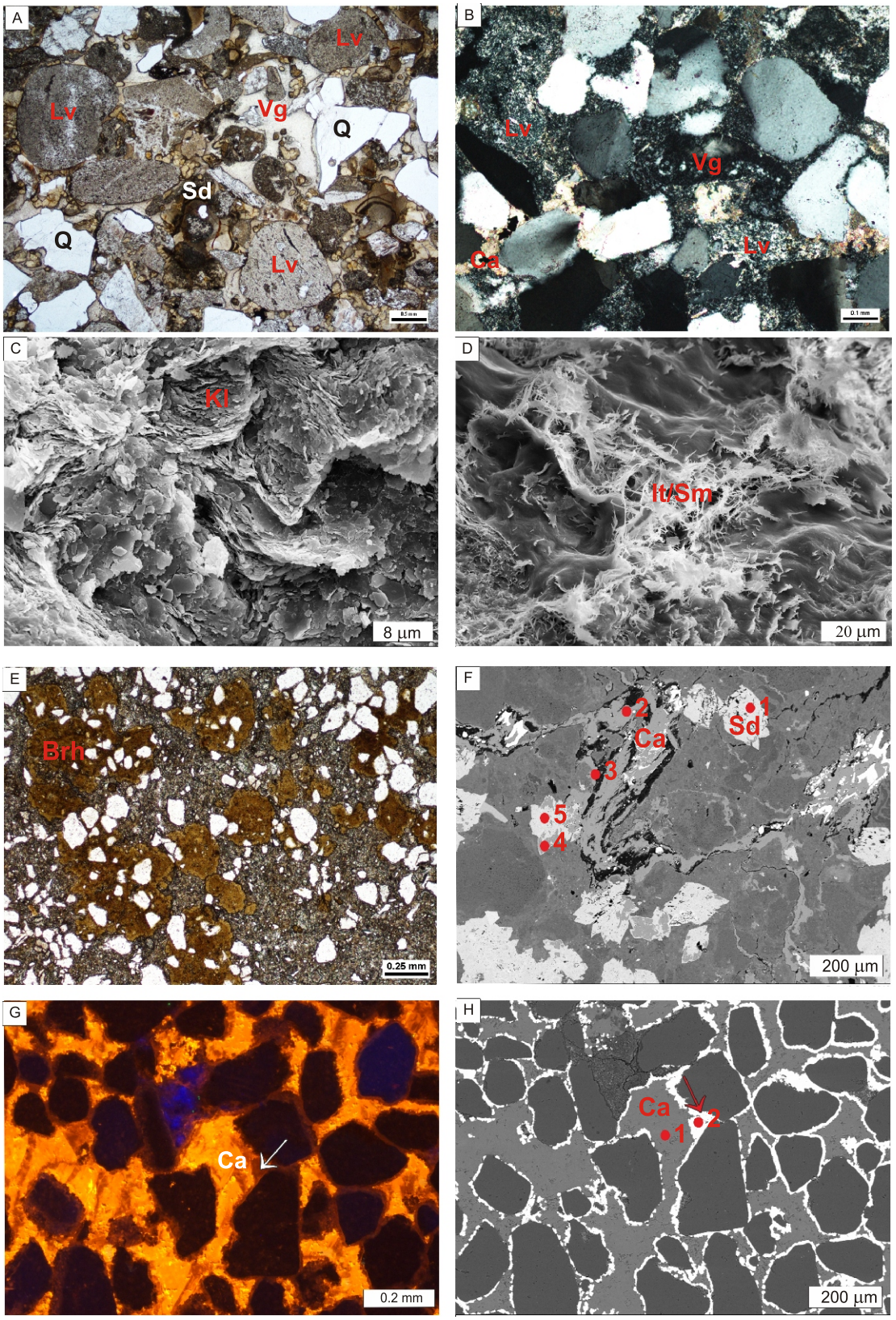

Fig. 11. Microphotographs taken in polarizing microscope, cathodoluminescence (CL) and scanning electron microscope (SEI, BSE)

A – coarse-grained volcaniclastic lithic arenite; numerous volcanic rock fragments (Lv); volcanic quartz grains (Q), siderite (Sd); Nasutów 1 borehole; depth 2162.35 m; sequence 3; without analyser; **B** – fine-grained volcaniclastic sublithic arenite cemented by calcite (Ca); volcanic rock fragments (Lv) type of rhyolite and volcanic glass (Vg); Zubowice IG 5 borehole; depth 1937.3 m; sequence 2; crossed polars; **C** – kaolinite (Kl) in the volcaniclastic sandstone; Łuków IG 5 borehole; depth 1203.5 m; sequence 3; SEI image; **D** – fibrous illite/smectite (It/Sm) mixed-layer minerals in volcaniclastic conglomerate; Niedrzwica IG 1 borehole; depth 2190.0 m; sequence 2; SEI image; **E** – fine-ash vitric-crystal tuff; oval forms like spherulites composed of berthierine (Brh); Korczmin IG 1 borehole; depth 1337.8 m; sequence 2; horizon 2.I; without analyser; **F** – carbonate minerals: calcite (Ca) and siderite (Sd) in fine-ash crystal tuff; 1-5 numbers – chemical analysis points (Table 7). Radzyń IG 1 borehole; depth 925.4 m; sequence 3; horizon 3.I, BSE image; **G** – carbonate minerals: calcite (Ca) with orange-yellow luminescence and lanthanum – neodymium carbonate (arrow) with brown-red luminescence in volcaniclastic sandstone; Korczmin IG 3 borehole, depth 1350.7 m, sequence 2, CL image; **H** – calcite (Ca) and lanthanum – neodymium carbonate (arrow) from Figure 11G;1, 2 numbers – chemical analysis points (Table 7); obraz BSE

Mineral and petrographic composition of the rocks studied with their lithofacies and sequence stratigraphic affiliations, and correlation horizons of the Upper Visean deposits (sequences 2, 3) in the Lublin Basin

BOREHOLE	SEQUENCE STRATIGRAPHY/ CORRELATION HORIZON	DEPTH [M]	TYPE OF ROCK/ LITHOFACIES	GRAIN AND MINERAL COMPOSITION	COMPOSITION OF CEMENT	STUDIES			
						PL	CL	SEM	XRD
NE region									
Łuków IG 4	2/ 2.I	1545.50	fine-ash vitric tuff, sideritized/T	volcanic glass pseudomorphs, volcanic quartz, rhyolite, trachyte, anatase, organic matter	kaolinite, siderite, calcite veins	+	+	+	
	2	1546.40 1546.90	fine-grained volcaniclastic polymictic orthoconglomerate/Gm	rhyolite, volcanic glass, volcanic quartz, anatase	siderite, kaolinite	+			
	2	1546.70	fine-grained volcaniclastic polymictic orthoconglomerate /Gm	rhyolite, basalt, volcanic glass, volcanic quartz, anatase, organic matter	kaolinite, chlorite, sandy matrix	+			
Łuków IG 5	3/ 3.I	1202.10	fine-ash vitric tuff/T	volcanic quartz, volcanic glass pseudomorphs, anatase, zircon	kaolinite, hematite	+			+
	3	1203.50	fine-grained volcaniclastic quartz wacke/Sh2	volcanic quartz, volcanic glass pseudomorphs, anatase, zircon	kaolinite, calcite, siderite	+		+	+
	2/ 2.I	1205.10 1206.75	fine-ash vitric tuff/T	volcanic quartz, volcanic glass pseudomorphs, muscovite, anatase	kaolinite>illite/smectite, hematite, siderite	+ +			+
	2	1209.40	fine-grained volcaniclastic quartz wacke/Sm	volcanic quartz, volcanic glass pseudomorphs, anatase, muscovite	kaolinite, siderite, calcite	+	+		
Radzyń IG 1	3/ 3.I	925.40	fine-ash vitric tuff, sideritized/T	apatite, anatase, pieces of organic matter	kaolinite>serpentine, siderite, calcite	+	+	+	+
	3/ 3.I	926.00 926.70	fine-ash vitric tuff, sideritized/T	bioclast fragments, anatase	kaolinite, serpentine siderite, calcite	+	+	+	
	3/ 3.I	927.70	coarse-ash vitric-lithic tuff/T	andesite, trachyte, basalt, rhyolite, volcanic glass, volcanic glass pseudomorphs, feldspar, zircon, anatase	calcite, hematite, serpentine, kaolinite	+			
	2/ 2.I	936.20	coarse-ash vitric tuff, heavily altered/T	volcanic glass pseudomorphs, volcanic glass, rhyolite, volcanic quartz, anatase	kaolinite, siderite, calcite, hematite, serpentine	+			
Central region									
Glinnik 2	3/ 3.I	2256.20 2257.35	fine-ash vitric tuff, perlitic texture/T	volcanic glass pseudomorphs, quartz, anatase	illite/smectite, illite, kaolinite, serpentine, siderite	+ +	+	+	+
Nasutów 1	3	2162.35	coarse-grained volcaniclastic lithic arenite/SGm	rhyolite, trachyte, andesite, volcanic glass, volcanic glass pseudomorphs, volcanic quartz, feldspar, anatase	siderite, kaolinite, illite/smectite, silica	+	+	+	
	3	2174.10	medium-grained volcaniclastic sublithic arenite/SGm	rhyolite, trachyte, andesite, tuff, volcanic glass pseudomorphs, volcanic quartz, feldspar, biotite, anatase	sideryt, kaolinit, illit/smectite, chlorite, silica	+			
	2/ 2.II	2186.20	fine-ash vitric tuff, vesicular texture/T	pumice, volcanic glass pseudomorphs	kaolinite>serpentine, illite/smectite, siderite, pyrite	+			+
	2/ 2.II	2186.30	fine-ash vitric tuff, fluidal texture/T	pumice, volcanic glass pseudomorphs	kaolinite>illite/smectite, serpentine, siderite, hematite	+	+	+	
	2/ 2.II	2188.20	fine-ash vitric tuff, fluidal texture/T	pumice, volcanic glass pseudomorphs	chalcedony, hematite, kaolinite> serpentine, siderite,	+			
Świdnik 22	3	1387.25	sandy, volcaniclastic mudstone/FSm	volcanic quartz, volcanic glass pseudomorphs, feldspar, muscovite, biotite, anatase, organic matter	siderite, kaolinite, illite	+			

Tabl. 4 cont.

	2/ 2.II	1396.20	fine-ash vitric-crystal tuff/T	volcanic quartz, feldspar, micas, anatase	kaolinite, illite/smectite, illite> serpentine, siderite	+			+
				SW region					
Niedrzwica IG 1	2	2190.00 2191.60	very fine-grained volcaniclastic polymictic orthoconglomerate/GSm	volcanic quartz, rhyolite, basalt, volcanic glass pseudomorphs, feldspar, zircon	sandy-clay-silica matrix, illite/smectite >90% illite, chlorite, siderite, hematite	+ +		+	+
				SE region					
Marynin 1	2	1353.60	sandy, volcaniclastic mudstone – *Stigmaria* soil/R	volcanic quartz, feldspar, volcanic rocks, volcanic glass pseudomorphs, muscovite, biotite, anatase, rutile	kaolinite, illite/smectite > illite, serpentine, pyrite, hematite	+		+	+
	2/ 2.I	1354.20	fine-ash vitric tuff, sideritized/T	volcanic glass pseudomorphs, volcanic quartz	siderite, kaolinite, illite/smectite, illite, serpentine	+	+	+	
Zubowice IG 5	2	1937.30	fine-grained volcaniclastic sublithic arenite/Sm	volcanic quartz, rhyolite, andesite, feldspar, volcanic glass pseudomorphs, micas	kaolinite, illite, serpentine, chalcedony, calcite, rhodochrosite, pyrite, calcite veins	+		+	
Terebin IG 1	2/ 2.I	1337.80	fine-ash vitric-crystal tuff, fluidal texture/T	volcanic quartz, muscovite, bioclast, organic matter	kaolinite, illite, pyrite	+			
Korczmin IG 1	2/ 2.I	1333.00	fine-ash vitric-crystal tuff T	volcanic quartz, anatase	kaolinite > illite/smectite, serpentine, hematite, pyrite	+		+	+
	2/ 2.I	1337.80	fine-ash vitric-crystal tuff, amygdaloidal/T	volcanic quartz, anatase, volcanic glass pseudomorphs	illite, chlorite, kaolinite, calcite	+		+	
	2	1339.60	medium-grained volcaniclastic quartz wacke, amygdaloidal/Sh2	volcanic quartz, feldspar, volcanic glass pseudomorphs, anatase	kaolinite, chlorite, illite, calcite, quartz, calcite veins	+	+		
Korczmin IG 3	2/ 2.I	1350.10	fine-ash vitric-crystal tuff/T	volcanic quartz, volcanic glass pseudomorphs, anatase,	kaolinite > illite/smectite, pyrite	+			+
	2	1350.70	very fine-grained volcaniclastic quartz wacke/Sm	volcanic quartz, feldspar, volcanic glass pseudomorphs, anatase	kaolinite, illite/smectite, calcite, lanthanum and neodymium carbonate	+	+	+	

SEQUENCE 2

Among the tuffs of sequence 2 (horizon 2.I and 2.II; Table 4), fine-ash vitric and vitric-crystal tuffs and coarse-ash vitric tuffs have been recognized (Figs. 10A, B, D, E and 11E). They are accompanied by volcaniclastic conglomerates, sandstones and mudstones (Figs. 10G, H and 11B, D, G, H).

TUFFS

Fine- and coars-ash vitric tuffs have been found in horizon 2.I in the NE region (Łuków IG 4, Łuków IG 5, Radzyń IG 1 boreholes) (Fig. 10A) and the SE region (Marynin 1 borehole) (Fig. 10D), and in horizon 2.II in the Nasutów 1 borehole (central region) (Fig. 10B). The fabric of the rock is unoriented or slightly directional, fluidal. The groundmass, originally glassy silt-grade, is composed of clay minerals, mainly kaolinite and minor mixed-layered illite/smectite minerals and serpentine, as confirmed by XRD. Some of the tuff has a significant proportion of chalcedony (Nasutów 1, depth 2188.20 m). It contains volcanic quartz grains (angular, embayed), whose content varies from a few to 20% by rock volume (Radzyń IG 1, Nasutów 1 boreholes), fragments of pumice – fiamme (black, flattened) (2I, NE region), volcanic glass altered into clay minerals and single volcanic rock clasts, and significant amounts of anatase and zircon. Additionaly some muscovite flakes and organic matter are also observed (2I, NE region). Oval forms composed of kaolinite, occasionally with serpentine in their outer parts, are visible in places (Nasutów 1, depth 2186.30 m). Tuff from the Marynin 1 borehole contains elongated, flattened fragments of volcanic glass that has undergone argillitization and silicification. The amount of siderite and sideroplesite is variable, and it is represented mainly by radial spherulites with an average size of ~0.05–3 mm, or irregular forms. In the Łuków IG 4 borehole, the tuff is sideritized. Calcite, mainly Fe/Mn-calcite, is present in smaller amounts and either forms nested clusters or fills fractures. The rock is cut by a network of irregular, dense fractures filled with iron oxides and hydroxides. Tuffs, which contain hematite and iron hydroxides, give the rock a red and in places yellow colour (Fig. 10A).

Fine-ash vitric-crystal tuff has been identified in horizon 2.I in the SE region in the following boreholes: Terebin IG 1, Korczmin IG 1 and Korczmin IG 3 (Fig. 10E and 11E) and in horizon 2.II from the Świdnik 22 borehole (central region). The rock exhibits a directional, fluidal fabric accentuated by the arrangement of clay mineral and mica flakes, clusters of organic matter, pyrite and, additionally, bioclast fragments in the Terebin IG 1 borehole, or an unoriented fabric (Świdnik 22 borehole). The rock is composed of volcanic ash and glass altered into clay minerals: kaolinite, mixed-layered illite/smectite minerals, illite, and serpentine or chlorites. The content of silt-grade (locally psammitic) detrital material is variable and ranges from a few to 40 vol.% of the rock. This material is angular and subrounded, poorly sorted. Monocrystalline quartz grains, single feldspar grains, muscovite flakes, and accessory minerals (zircon and anatase) are found. Organic matter forms small lenses (2.II, central region). Tuff

from the Terebin IG 1 borehole contains bioclasts (bivalve shells, echinoderm skeletal fragments). Some voids within the bioclasts are filled with kaolinite, and pyritization is visible in places. Tuff from the Korczmin IG 1 borehole reveals the presence of amygdaloidal, irregular forms, slightly flattened, bent, and filled with quartz or, on the outside, with chlorite and, on the inside, with Fe/Mn-calcite and quartz. In addition, there are numerous oval ooid-like forms of slightly concentric structure, composed of a brown clay mineral (serpentine – berthierine) (Fig. 11E) and irregular dark clusters of hematite. In places, pyrite is present in the tuffs (Terebin IG 1, Korczmin IG 1 boreholes). Carbonates are represented by siderite showing irregular forms (Świdnik 22 borehole). Calcite fills veins or has formed by replacement of other minerals (Korczmin IG 1 borehole).

VOLCANICLASTIC ROCKS

Fine-grained volcaniclastic polymictic orthoconglomerates have been found in NE region (lithofacies Gm; Łuków IG 4 borehole) (Fig. 10G) and the SW region (lithofacies GSm; Niedrzwica IG 1 borehole) (Fig. 10H). The fabric of the rock is unoriented or oriented, emphasised by the arrangement of rock clasts, organic matter and clay minerals. The content of material with diameter >2 mm (20 mm and 2.2 mm respectively most frequent) is ~ 35–80%. These are rounded and subrounded clasts of volcanic rock, largely of rhyolite type, fragments of volcanic glass and volcanic quartz grains (Table 4). The volcanic rocks and glass exhibit common effects of argillitization, silicification and carbonatization processes. Psephitic detrital material is bonded by a sand-mud-clay matrix and by cement. In the sand-silt fraction, there are poorly rounded, angular (mainly monocrystalline) quartz grains. The additional constituents are rock clasts (volcanic rocks, quartzites, very fine-grained sandstone, mudstones, granitoid) and feldspars. Anatase is common; locally zircon is present. The content of muscovite flakes (muscovite) and organic matter is low. The effects of calcitization, kaolinitization and hematitization processes are common in the feldspars. Clay minerals are represented by kaolinite, mixed-layered illite/smectite minerals (Fig. 11D), illite, serpentine and chlorite. Carbonate minerals are represented by siderite and sideroplesite; fine radial spherulites with an average size of ~0.08 mm are present in the Łuków IG 4 borehole. In addition to those, sulphides, mainly pyrite, are also present.

Very fine- to medium-grained volcaniclastic quartz wackes have been identified in the NE region (Łuków IG 5 borehole) and the SE region (Korczmin IG 1, Korczmin IG 3 boreholes). They belong to lithofacies Sm (Łuków IG 5, Korczmin IG 1 boreholes) and lithofacies Sh2 (Korczmin IG 3 borehole). Detrital material is subrounded and angular, and the sorting is variable. The main component of the grain framework is monocrystalline quartz, many grains being of volcanic origin (angular, embayed). There are also fragments of volcanic glass, feldspar grains and muscovite flakes. Some of these have undergone processes of kaolinitization, argillitization, chloritization and carbonatization. Accessory minerals comprise anatase, rutile and zircon. Sandstone from the Korczmin IG 1 borehole contains irregularly shaped, slightly flattened, bent amygdaloidal forms filled with silica, or with chlorite on the outside and with Fe/Mn-calcite and quartz on the inside. The binder is represented by clay minerals: kaolinite, mixed-layered illite/smectite minerals, chlorites and carbonate minerals (siderite and calcite) (Fig. 11G, H). The other constituents found in the sandstone from the Korczmin IG 3 borehole are lanthanum and niobium carbonate, forming rims on detrital grains (Fig. 11G, H). This mineral could belong to the bastnäsite or hydroxylbastnäsite mineral group. Furthermore, in the sandstone from the Korczmin IG 1 borehole, overgrowths of quartz cement are visible on quartz grains.

Fine-grained volcaniclastic sublithic arenite (lithofacies Sm), has been identified (Fig. 11B) in the Zubowice IG 5 borehole. The rock exhibits an unoriented fabric. The main mineral component of the grain framework comprises subrounded and angular quartz grains (some of volcaniclastic origin). Feldspars are represented by plagioclase and potassium feldspars, which show the effects of processes of argillitization, albitization, and replacement by calcite. The most common mica mineral in the rocks is biotite. Lithoclasts are dominated by pieces of volcanic acidic rock of rhyolite type and deformed and stretched fragments of volcanic glass (argillitization, calcitization). The sandstones are cemented by carbonates (Fe/Mn-calcite, ankerite), clay minerals (kaolinite, illite, serpentine) and chalcedony. Pyrite forms larger aggregations. The sandstone is cut by thin calcite veins.

Volcaniclastic sandy mudstone (*Stigmaria* soil, lithofacies R) has been recognized in SE region (Marynin 1 borehole). The rock is characterized by a slightly oriented fabric accentuated by the arrangement of irregular lenses enriched in clay minerals, organic matter and pyrite. The grains are angular and poorly sorted. The grain framework is composed of quartz (mainly monocrystalline), feldspars, fragments of volcanic rock and volcanic glass, micas (muscovite, biotite) and accessory minerals: anatase, rutile and zircon. The rock fragments and feldspars show the effects of argillitization. The groundmass is made up of clay minerals, among which there are, in similar amounts, kaolinite and mixed-layered illite/smectite minerals, and small quantities of serpentine and illite. Pyrite crystals are concentrated in the form of laminae, lenses and irregular bodies.

SEQUENCE 3

Sequence 3 hosts fine-ash vitric and coarse-ash vitric-lithic tuffs (Figs. 10C, F and 11F) in the NE and central regions (Table 4). They are accompanied by volcaniclastic rocks: sandstones and mudstones (Fig. 11A, C).

TUFFS

Fine-ash vitric tuffs have been found in horizon 3.I in the NE region (Łuków IG 5, Radzyń IG 1 boreholes) and in the central region (Glinnik 2 borehole; Fig. 10C). Their fabric is unoriented or slightly directional and fluidal, manifested by the linear arrangement of organic matter and hematite. The rocks are composed of ash and volcanic glass altered into clay minerals, mainly kaolinite, mixed-layered illite/smectite minerals, illite (muscovite 2M1) and serpentine (Table 5). The content of detrital material varies from a few to 20 vol.% of the rock (Łuków IG 5 borehole). There are also angular volcanic quartz grains of the silty or sandy fractions, volcanic glass, sparse feldspar grains, muscovite flakes, as well as anatase and apatite, locally found in significant amounts (Radzyń IG 1, depth 925.4 m, Table 5). Fragments of bioclasts (including bivalve shells, depths 926.7–925.4 m), whose frequency decreases upwards, are visible in tuffs from the Radzyń IG 1 borehole. Carbonate minerals are represented by siderite and calcite (Figs. 10C and 11F). Siderite occurs as radial spherulites with an average size of ~0.7–0.12 mm or irregular, oval specimens. Fe/Mn-calcite creates fine rhombohedral and other forms. In places, the tuffs are cut by irregular calcite veinlets. In tuffs from the NE region hematite and iron hydroxides are present, which give the rock red and in places yellow colours.

Table 5

XRD analyses

BOREHOLE	SEQUENCE STRATIGRAPHY/ CORRELATION HORIZON	DEPTH [M]	TYPE OF ROCK/ LITHOFACIES	QUARTZ	PLAGIO-CLASE	CALCITE	SIDERITE	PYRITE	JARO-SITE	HEMA-TITE	APATITE	ANATASE	RUTILE	KAOLINITE*/	MUSCO-VITE 2M1	ILLITE-SMECTITE **	SERPEN-TINE	% AL_2O_3
	NE region																	
Łuków IG 5	3/ 3.I	1202.10	fine-ash vitric tuff/T	26.6						2.7		1.0		69.7 (HI = 0.41)				28
	3	1203.50	fine-grained volcaniclastic quartz wacke /Sh2	75.7		1.3	0.5					0.3		22.2 (HI = 0.87)				9
	2/ 2.I	1206.75	fine-ash vitric tuff/T	6.4						5.5		1.1		81.5 (HI = 0.38)		5.5		32
Radzyń IG 1	3/ 3.I	925.40	fine-ash tuff, sideritized/T	0.6		1.5	17.0				12.2	9.6		50.1 (HI = 1.86)			9.0	20
	Central region																	
Glinnik 2	3/ 3.I	2257.35	fine-ash vitric tuff, perlitic texture/T	25.4			2.0					0.4		18.8	14.2	33.4	5.8	7
Nasutów 1	2/ 2.II	2186.20	fine-ash vitric tuff, vesicular texture/T	0.3			1.9					0.9		88.2 (HI = 1.17)		3.4	5.3	35
Świdnik 22	2/ 2.II	1396.20	fine-ash vitric-crystal tuff/T	16.7	3.1		2.1					0.8		36.9	16.4	21.2	2.8	15
	SE region																	
Marynin 1	2	1353.60	sandy, volcaniclastic siltstone – *Stigmaria* soil/R	45.3	1.0			2.8	2.0			0.8	0.4	20.9	5.5	19.3	2.0	8
Korczmin IG 1	2/ 2.I	1333.00	fine-ash vitric-crystal tuff/T	26.2				5.8	5.2	1.5		0.2		47.8 (HI = 0.27)		8.9	4.4	19
Korczmin IG 3	2/ 2.I	1350.10	fine-ash vitric-crystal tuff/T	65.8				1.9	2.2					20.5 (HI = 0.59)		9.6		8

* HI – indicates Hinckley index – calculations for samples containing clay minerals other than kaolinite should be considered with caution. HI was calculated only for samples dominated by kaolinite as a clay mineral; ** Ilite-smectite contains a significant amount of illite packets (%illite > 75%); the exception is a sample from Świdnik 22, which may contain more smectite.

Coarse-ash vitric-lithic tuff from the Radzyń IG 1 borehole (NE region) occurs below the fine-ash vitric tuffs (Fig. 10F); both together form the fining-upwards horizon 3.I. The fabric of the rock is slightly directional, manifested by the linear arrangement of grains. The rock is composed mainly of fragments of volcanic rock (andesite, trachyte, basalt, rhyolite) and glass, in which the effects of kaolinization, serpentinization and silicification processes are visible. Anatase and zircon are also present. The grain material is cemented by kaolinite and serpentine, which are products of alteration of volcanic dust and glass, and by Fe/Mn-calcite and hematite.

VOLCANICLASTIC ROCKS

Fine-grained volcaniclastic quartz wacke (lithofacies Sh2) has been identified in the NE region (Łuków IG 5 borehole). The rock is characterized by an unoriented fabric. The detrital material is subrounded and angular. Predominant are quartz grains, mainly monocrystalline, commonly angular, of volcanic origin. There are also frequent fragments of volcanic glass, stretched, deformed and altered into mainly kaolinite and less commonly into mixed-layered illite/smectite minerals, potassium feldspar grains, and muscovite flakes. Accessory minerals are represented by anatase, rutile and zircon. The binder is composed of kaolinite (Fig. 11C) (being a product of alteration of volcanic glass), siderite cement forming nested and locally oval concentrations, and calcite.

Medium-grained (Sm) and coarse-grained volcaniclastic lithic arenite (lithofacies SGm) (Fig. 11A) has been identified in the central region (Nasutów 1 borehole). The rock exhibits an unoriented fabric. Detrital material is poorly rounded and poorly sorted. The grain framework is composed of lithoclasts, feldspars and quartz. Rock fragments represent effusive rocks mainly of rhyolite type, less frequently of trachyte or andesite types, fragments of volcanic glass, and tuff. The effects of silicification, argillitization, chloritization and carbonatization are commonly observed. Feldspars are represented by potassic feldspars and plagioclases, which commonly show the effects of kaolinitization, argillitization, albitization and carbonatization. Quartz grains are predominantly of volcanic origin (embayed, angular). Single flakes of biotite are visible. Anatase and zircon are present in abundance. Granular material is cemented by siderite, which is represented by very finely crystalline and massive forms, and by fine spherulites, ~0.02 mm in size. In addition, there are clay minerals being the product of alteration of volcanic glass. These are mainly kaolinite, mixed-layered illite/smectite minerals, and chlorite. Iron hydroxides and pyrite are present in dispersed form.

Volcaniclastic sandy mudstone (lithofacies FSm) is present in the central region (Świdnik 22 borehole). Its directional fabric is accentuated by the arrangement of micritic siderite, laminae or fragments of organic matter, and mica flakes. Most of the silt- and sand-grade detrital material is represented by subrounded and angular (volcaniclastic) quartz grains. Quartz is mostly monocrystalline. The other constituents are feldspars, some of which are completely altered into kaolinite (kaolinite pseudomorphs). Volcanic rock clasts are sparse, while fragments of volcanic glass are abundant. They show the effects of argillitization and silicification. Muscovite and biotite flakes are present in small amounts. Sulphides (probably pyrite) occur in association with organic matter; zircon and anatase were also observed. The cement consists of clay minerals and siderite.

MINERALOGY

CLAY MINERALS

Clay minerals are the main component of the tuffs and form part of the cements in the volcaniclastic sandstones and conglomerates. Among the clay minerals, kaolinite, muscovite 2M1, mixed-layered illite/smectite minerals, and serpentine have been distinguished (Table 5). Kaolinite is the most common mineral in the rocks studied (Figs. 10A and 11C) and was found by XRD in amounts from 19 to 88%. Vermiform kaolinite shows oval forms in places, which likely either developed as a result of gas bubble filling or are the product of alteration of feldspar grains and fragments of volcanic glass. Mixed-layered illite/smectite minerals (containing >75% of illite – having basal spacing close to 10 Å) commonly co-occur with kaolinite and can be found at up to 33%. Illite (muscovite 2M1) and serpentine are found in much smaller amounts (up to 16 and 9%, respectively). Locally, oval forms composed of serpentine – berthierine were observed (Fig. 11E). Trioctahedal structure is confirmed by positions of the (020) and (060) reflections, at 4.68 Å and 1.55 Å, respectively. Berthierine presence is suggested by polytype 1M visible as a reflection at 2.67–2.69 Å (Toth and Fritz, 1997; Fig. 12). Chrysotile is predominantly monoclinic, but it lacks a reflection at 2.67–2.69 Å (Falini et al., 2004), while lizardite crystallises as polytypes 1T and 2H1, and also it lacks this reflection. Chemical analyses performed on several samples of this mineral confirm that this is berthierine (Table 6), as it shows substantial amount of iron relative to magnesium.

The volcaniclastic sandstones and conglomerates contain vermiform kaolinite, fibrous illite, mixed-layered illite/smectite minerals (Fig. 11D), and pseudohexagonal chlorite crystals. These minerals crystallized in pore voids or formed by the alteration of feldspar grains, fragments of volcanic glass, and lithoclasts.

The X-ray diffraction data was used to calculate the Hinckley index (HI), used to evaluate kaolinite disorder. It is calculated based on the equation:

$$HI \quad \frac{B \quad C}{A}$$

where: A – the height of the (1–10) reflection, measured from the general background; $(B + C)$ – the sum of intensities of the (1–10) and (11–1) peaks measured from the inner-peak background (Fig. 13).

According to Zadvernyuk et al. (2021) HI = 0.7 can be considered as a boundary between kaolinite of dominantly primary origin, and secondarily formed via destruction of crystals due to transportation and deposition. A similar observation was made by Oyebanjo et al. (2018), who found that kaolinite from sandstones has a lower HI than from pure kaolin. Moreover, Liu et al. (2022) reported that kaolinite crystallinity correlates positively with its clay mineral content, purity and particle size.

Analysis of the HI results obtained indicates that there is no spatial correlation between HI and location. For example, samples from the Łuków IG 5 and Radzyń IG 1 boreholes, despite being located close to each other, have significantly different HI values. Similarly, there is also no correlation between HI and

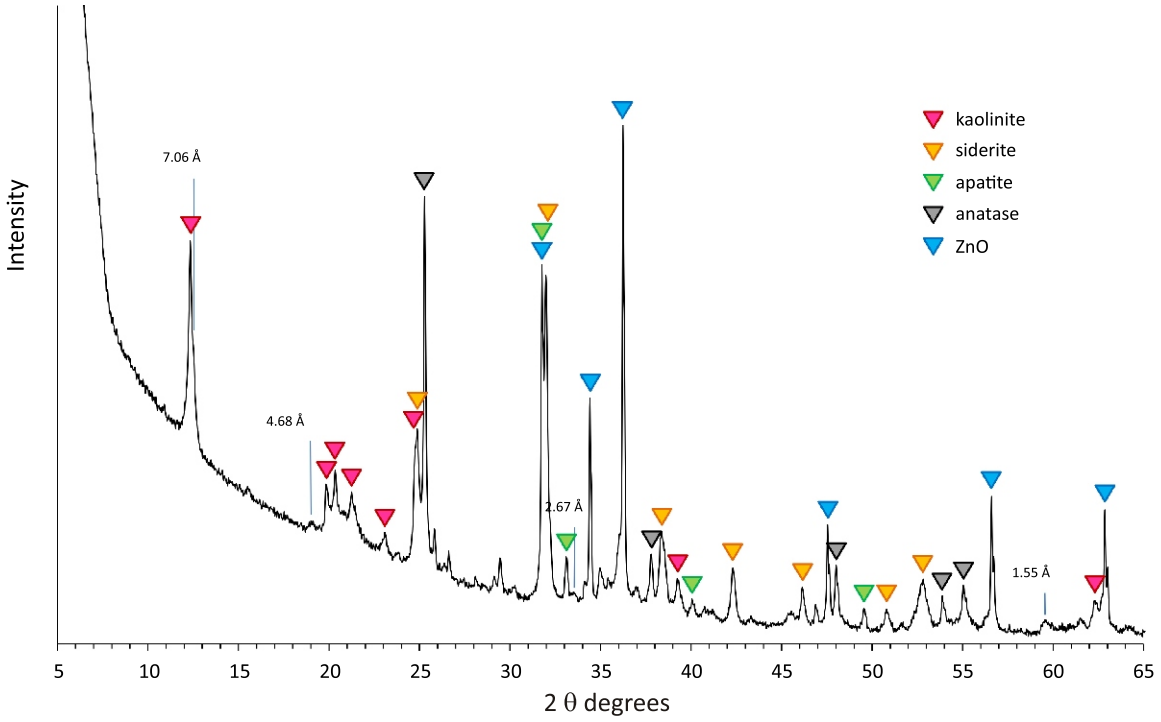

Fig. 12. XRD diagram of tuff with characteristic reflections of berthierine; Radzyń IG 1 borehole; depth 925.40 m; sequence 3; correlation horizon 3.I

the stratigraphic position of these samples in the profile. This suggests that the degree of ordering of kaolinite in the samples analysed should be related to local transformation of kaolinite, due to interaction with hydrothermal fluids and limited transport and sedimentation. In fluvial floodplain and deltaic plain settings, reworking and lateral transport of fine volcanic material could occur, potentially leading to partial redeposition (e.g., samples from the Łuków IG 5 borehole). By contrast, shallow-water delta and clay shelf environments more likely preserve tuffaceous material close to its original depositional position, with diagenetic alteration occurring *in situ*, as in the case of the Radzyń IG 1 sample, which has the highest HI. This sample contains also the highest content of siderite and apatite, and could not have been redeposited. In the remaining samples, less advanced weathering or minor redeposition could explain the lower degree of kaolinite disorder.

CARBONATE MINERALS

Carbonate minerals (Table 7) are represented by siderite and sideroplesite (minerals of the siderite-magnesite isomorphic series), and by calcite; ankerite and a carbonate that contains lanthanide group elements are found locally.

Siderite and sideroplesite occur as spherulites, incompletely developed forms resembling spherulites or rhombohedral crystals, and as very finely crystalline cement. Spherulites and spherulite-like forms are common in the tuffs (Figs. 10C, F and 11F). The average size of the spherulites ranges from 0.02 to 3 mm. Central parts of the spherulites and rhombohedral crystals are often composed of siderite, while their outer parts consist of sideroplesite. Very finely crystalline siderite and sideroplesite most often form cement in the volcaniclastic sandstones (Fig. 11A) and conglomerates. The

Table 6

Chemical composition of berthierine based on microprobe analyses

BOREHOLE TYPE OF ROCK / CORRELATION HORIZON	DEPTH [m]	SiO_2 (wt.%)	Al_2O_3 (wt.%)	FeO (wt.%)	MNO (wt.%)	CaO (wt.%)	MgO (wt.%)	K_2O (wt.%)	TiO_2 (wt.%)	Total (wt.%)
NE REGION										
Radzyń IG 1 coarse-ash vitric-lithic tuff/ 3.I	927.70	22.42	21.10	30.53	0.27	0.40	2.02	0.00	2.29	79.03
		22.58	22.46	29.95	0.14	0.22	2.22	0.00	1.12	78.65
CENTRAL REGION										
Glinnik 2 fine-ash vitric tuff/ 3.I	2257.35	28.34	21.29	34.00	0.09	0.28	2.55	0.77	0.01	87.33
		29.19	21.44	33.81	0.13	0.17	2.38	0.67	0.11	87.90
		35.37	23.66	23.72	0.00	9.29	1.80	2.24	0.44	87.53
		34.76	23.08	24.54	0.00	0.37	1.69	1.65	0.35	86.44
SE REGION										
Korczmin IG 1 fine-ash vitric-crystal tuff/ 2.I	1337.80	27.88	21.13	31.64	0.00	0.19	7.61	0.07	0.13	88.65
		28.46	21.41	31.15	0.00	0.18	7.45	0.00	0.11	88.75
		27.28	20.55	31.17	0.00	0.03	7.41	0.00	0.22	86.67

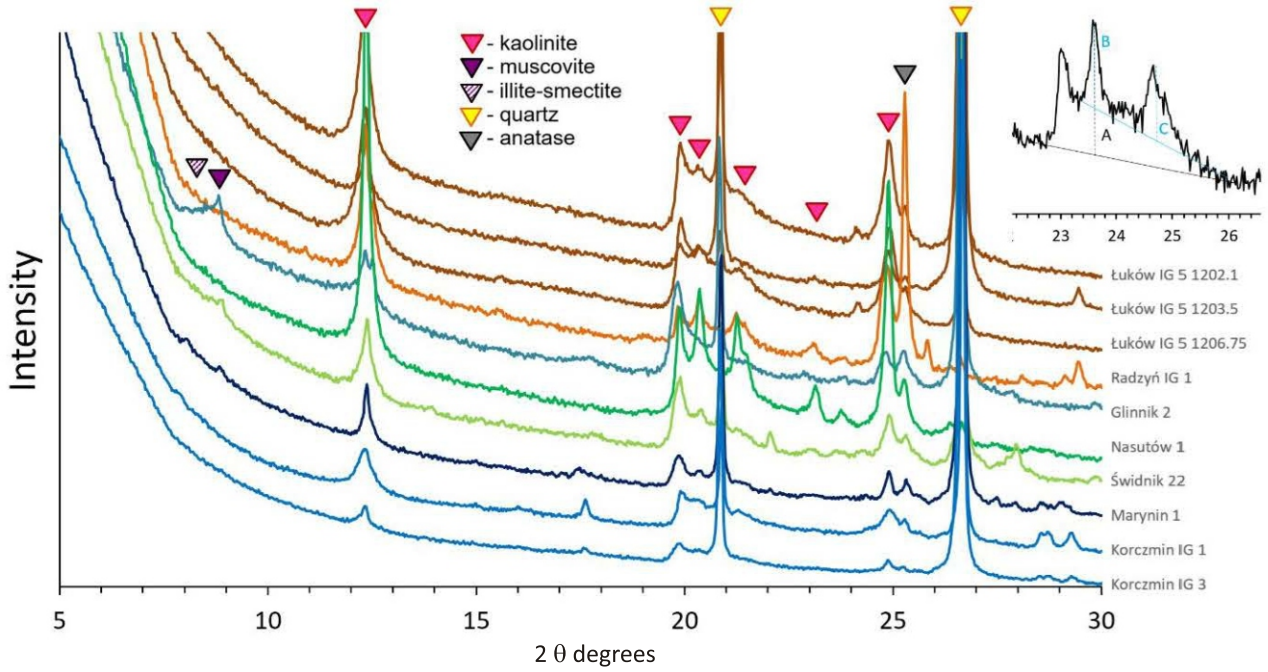

Fig. 13. Diffractograms of the samples studied with peaks of kaolinite, for which the Hinckley Crystallinity Index was calculated (methodology of calculations is shown in small inset in upper-right part)

average chemical composition of the siderite is as follows: 97.2–99.9 mol% $FeCO_3$, 0–3.4 mol% $MgCO_3$, 0.1–1.4 mol% $CaCO_3$, and 0–1.4 mol% $MnCO_3$, and of the sideroplesite: 71.1–93.3 mol% $FeCO_3$, 3.4–18.9 mol% $MgCO_3$, 0.9–7.4 mol% $CaCO_3$, and 0.2–5.8 mol% $MnCO_3$ (Table 7).

Calcite occurs as cement; it fills voids in the rock (fractures, amygdaloidal forms) and replaces grains (Fig. 11B, F–H). Occasionally, calcite is developed as rhombohedral crystals. This mineral represents varieties enriched in iron and manganese, with different ratios of one element to the other. This affects the colour of calcite (ranging from yellow and orange to red) in cathodoluminescence (Fig. 11G). When manganese predominates over iron, the colour is closer to yellow, while in the opposite situation it is closer to red. The average chemical composition of the calcite is as follows: 93.4–99.3 mol% $CaCO_3$, 0.7–3.4 mol% $FeCO_3$, 0–1.9 mol% $MgCO_3$, and 0–1.8 mol% $MnCO_3$ (Table 7).

Ankerite is present in volcaniclastic sandstone from the Zubowice IG 5 borehole, as one of the cement components in the rock. Its presence was confirmed by cathodoluminescence (it is non-luminescent) and by spot chemical analysis (Table 7).

Rare earth carbonate, containing elements of the lanthanide group, has been identified in volcaniclastic sandstone of the Korczmin IG 3 borehole (depth 1350.7 m) (Fig. 11G, H). The mineral forms rims on detrital grains, in places filling the pore space completely. Spot chemical analyses, performed by microprobe of a scanning electron microscope, show the following contents:

- point 2 – 42.60 wt.% CO_2, 24.12 wt.% La_2O_3, 16.96 wt.% Nd_2O_3, 4.71 wt.% Pr_2O_3, 0.84 wt.% Y_2O_3, 0.46 wt.% CaO;
- point 3 – 41.71 wt.% CO_2, 13.89 wt.% La_2O_3, 12.14 wt.% Nd_2O_3, 5.37 wt.% Ce_2O_3, 3.40 wt.% Pr_2O_3, 2.44 wt.% Y_2O_3, 15.57 wt.% CaO.

ANATASE AND RUTILE

Anatase is a common mineral whose average content in the rocks is ~1%, maximally ~10 % (Table 5). It forms subhedral and euhedral crystals dispersed in the clay groundmass or precipitates in empty spaces (e.g., gas bubbles; Fig. 10F). Analyses of the chemical composition of anatase from tuff in the Radzyń IG 1 borehole (depth 927.7 m) indicate its enrichment in zircon, iron and niobium. The ZrO_2 content ranges from 1.13 to 3.51 wt.%, the maximum is >13 wt.%, while the FeO and Nb_2O_5 contents reach 1 wt.%. In places, anatase is accompanied by rutile.

APATITE

Large amounts of apatite (~12 wt.%; Table 5) have been identified in one tuff sample. It forms very small subhedral and euhedral crystals dispersed in the clay and carbonate groundmass.

PYRITE AND JAROSITE

In considerable quantities of up to ~6% (Table 5), pyrite occurs in tuffs of the south-eastern region. It usually forms cubic crystals that occasionally comprise larger aggregations (nests, lenses). Pyritization of bioclast fragments was observed locally. Pyrite is often accompanied by jarosite (up to ~ 5%, Table 5), a sulphate that is a product of pyrite oxidation.

HEMATITE

The tuffs contain hematite and poorly crystalline iron hydroxides. These minerals give the yellow-red-brown colour to the rocks and are dispersed or form lenticular clusters (Fig. 10A). In the volcaniclastic rocks, hematite replaces feldspar grains and rock clasts.

Table 7

Chemical composition of carbonates based on microprobe analyses

BOREHOLE	SEQUENCE STRATIGRAPHY/ CORRELATION HORIZON	DEPTH [M]	TYPE OF ROCK/ LITHOFACIES	POINT OF ANALYSIS	Mg wt.%	Ca wt.%	Mn wt.%	Fe wt.%	$MgCO_3$ mol%	$CaCO_3$ mol%	$MnCO_3$ mol%	$FeCO_3$ mol%	CARBONATE TYPE
NE region													
Łuków IG 4	2/ 2.I	1545.50	fine-ash vitric tuff, sideritized/T	1	0.15	38.84	0.63	0.54	0.5	97.1	1.3	1.1	Mn/Fe-calcite vein
				2	5.29	3.58	0.36	33.57	18.9	9.2	0.8	71.1	sideroplesite rhombohedra
				3	0.00	0.54	0.66	45.58	0.0	1.4	1.4	97.2	sideroplesite rhombohedra
				5	0.03	0.40	0.64	45.99	0.1	1.0	1.4	97.5	sideroplesite rhombohedra
				6	3.99	3.29	0.09	37.45	14.0	8.2	0.2	77.6	sideroplesite rhombohedra
Łuków IG 5	2	1209.40	fine-grained volcaniclastic quartz wacke/Sm	1	0.08	0.48	0.35	46.39	0.3	1.2	0.7	97.8	sideroplesite spherulite
				3	0.00	39.34	0.00	0.33	0.0	99.3	00	0.7	Fe-calcite
Radzyń IG 1	3/ 3.I	925.40	fine-ash vitric tuff, sideritized/T	1	1.58	1.05	1.43	42.68	5.5	2.6	3.0	88.9	sideroplesite spherulite
				2	0.22	38.99	0.34	0.60	0.8	97.3	0.7	1.2	Fe-calcite
				3	0.10	39.26	0.49	1.11	0.4	96.3	1.0	2.3	Fe/Mn-calcite
				4	0.16	37.91	0.43	1.45	0.6	95.5	0.9	3.0	Fe/Mn-calcite
				5	1.13	0.94	1.10	44.22	4.0	2.4	2.3	91.3	sideroplesite spherulite
	2/2.I	936.2	coarse-ash vitric tuff, heavily altered/T	1	0.20	39.64	0.50	0.71	0.7	96.8	1.0	1.5	Fe/Mn-calcite
				2	1.08	0.70	1.87	43.07	3.8	1.8	4.0	90.4	sideroplesite
Central region													
Nasutów 1	3	2162.35	coarse-grained volcaniclastic lithic arenite/Gm	1	0.98	2.12	0.59	43.53	3.4	5.3	1.2	90.1	sideroplesite rhombohedra
				2	3.59	3.09	0.00	40.47	12.1	7.4	0.0	80.5	sideroplesite rhombohedra
	2/2.II	2186.3	fine ash vitric tuff, fluidal texture/T	1	0.30	0.40	0.51	47.13	1.0	1.0	1.1	96.9	sideroplesite spherulite
				2	3.10	1.87	0.18	40.06	10.9	4.8	0.4	83.9	sideroplesite spherulite
SW region													
Niedrzwica IG 1	2	2191.6	very fine-grained volcaniclastic polymictic paraconglomerate/GSm	1	0.01	0.40	0.64	46.97	0.0	1.0	1.3	97.7	siderite
				2	2.46	1.50	2.22	39.97	8.6	3.8	4.6	83.0	sideroplesite
				3	4.27	0.35	2.75	37.79	14.9	0.9	5.8	78.4	sideroplesite
SE region													
Marynin 1	2	1354.2	fine-ash vitric tuff, sideritized/T	1	0.15	1.99	0.59	44.87	0.5	5.0	1.2	93.3	sideroplesite spherulite
				4	0.00	0.02	0.00	46.89	0.0	0.1	0.0	99.9	sideroplesite spherulite, cement
Korczmin IG 1	2	1339.6	medium-grained volcaniclastic quartz wacke, amygdaloidal/Sh2	1	0.24	38.57	0.00	1.12	0.8	96.9	0.0	2.3	Fe-calcite
				2	0.24	38.75	0.25	0.62	0.8	97.4	0.5	1.3	Fe-calcite
				3	0.57	38.83	0.56	0.64	1.9	95.6	1.2	1.3	Fe/Mn-calcite
				4	0.32	39.48	0.40	0.76	1.1	96.6	0.7	1.6	Fe/Mn-calcite
Korczmin IG 3	2	1350.7	very fine-grained volcaniclastic quartz wacke/Sm	1	0.20	38.73	0.77	0.34	0.7	98.0	1.6	0.7	Mn-calcite
Zubowice IG 5	2	1937.3	fine-grained volcaniclastic sublithic arenite/Sm	1	0.45	37.39	0.75	1.64	1.6	93.4	1.6	3.4	Fe/Mn-calcite
				2	0.23	38.84	0.84	0.70	0.8	95.0	1.8	1.4	Mn/Fe-calcite
				3	6.31	22.66	1.13	8.57	22.4	57.2	2.4	18.0	ankerite
				4	0.19	38.69	0.49	0.62	0.7	97.0	1.0	1.3	Fe/Mn-calcite

DISCUSSION

REGIONAL AND STRATIGRAPHIC VARIABILITY OF COMPOSITION OF ROCKS

In the Carboniferous section of the Lublin Basin, tuffs have been previously identified in a few boreholes, being reported from the Tournaisian and Visean by Popek (1986), Kozłowska and Popek (2018), Waksmundzka et al. (2021), Kozlowska and Waksmundzka (2023), and from the Bashkirian by Kozłowska (2023). The present study, based on data from many boreholes, has identified three new tuff horizons within the Upper Visean deposits (sequences 2 and 3). Because of their regional nature, as well as the possibility of correlation in borehole sections located in different parts of the Lublin Basin, they are considered good correlative horizons and designated with the symbols 2.I, 2.II and 3.I (Figs. 7–9 and Table 3).

Two tuff layers have been characterized within sequence 2: the lower tuff 2.I found in the NE and SE regions, and the upper tuff 2.II reported from the central and SE regions. Tuff 3.I occurs in sequence 3 and has been found so far in the NE and central regions. The dominant mineral in the composition of the tuffs is kaolinite, and its content can exceed 80% (Table 5). The average content of Al_2O_3 in tuffs 2.I, 2.II and 3.I was estimated at 28–35% (Łuków IG 5, Nasutów 1 boreholes), which is a prospective amount for the production of refractory materials (Szczerba, 2006). Searches for bauxite conducted in the 1970s and 1980s led to the documentation of a balance layer in the NE region of the basin (Parczew IG 10 borehole), but this was not pursued (Cebulak, 1978; Cebulak et al., 2011). Our preliminary pilot results indicate that tuff horizons may contain significant Al_2O_3, which indicates their bauxite prospectivity. These estimates should be regarded as preliminary and require further studies in terms of the raw material potential of the deposits in sequences 2 and 3.

Volcaniclastic conglomerates occur in the NE and SW regions, in sequence 2 immediately below tuff 2.I. Compared to the volcaniclastic conglomerates of sequence 1 (Tournaisian), previously characterized in publications by Waksmundzka et al. (2021) and Kozłowska and Waksmundzka (2023), in which clasts of volcanic rocks, i.e. rhyolite, trachyte, andesite, basalt and dacite, are present, the conglomerates of sequence 2 are conspicuous by a lower diversity of clast types. A similar relationship was also found both as regards the type of clay minerals, which are additionally represented by chlorite and illite in the conglomerates from sequence 1, and as regards the chemical composition of carbonates among which calcite and rhodochrosite are also present.

Volcaniclastic sandstones and sandy mudstones (including *Stigmaria* palaeosoil) occur in sequence 2 in the NE and SE regions, and in sequence 3 in the NE and central regions. In the borehole sections under study, the position of the sandstones is the same as that of the conglomerates, occurring beneath tuffs 2.I or 3.I. One of the mudstones developed as a *Stigmaria* palaeosoil directly underlies tuff 2.I., while the other occurs as an interbed within a thick claystone-mudstone interval in the lower part of sequence 3.

For the first time in the history of petrographic-mineralogical studies of the Carboniferous deposits in the Lublin Basin, rare earth minerals – lanthanum and neodymium carbonates – were identified in the cement of sandstone of sequence 2 from the SE region. Compared to the volcaniclastic sandstones of sequence 1 (Tournaisian) described in Waksmundzka et al. (2021) and Kozłowska and Waksmundzka (2023), quartz wackes were also identified among the sandstones of sequences 2 and 3, which do not contain clasts of volcanic rocks, but only fragments of volcaniclastic glass. The grain and mineral compositions of the sublithic and lithic arenites of sequences 2 and 3 correspond to those of sequence 1 sandstones.

Deposition of the volcaniclastic conglomerates and sandstones that fill the river channels and incised valleys located at the bottom of sequences 2 and 3 was preceded by erosion that took place during a forced regression and RSL lowstand. The eroded bedrock that underlies sequence 2 was represented by lithologies including basalts, tuffs, conglomerates and volcaniclastic sandstones included in sequence 1. The erosion preceding the accumulation of sequence 3 affected the deposits of sequence 2, including conglomerates and volcaniclastic sandstones and tuffs that are present in the bedrock. Therefore, it appears that the detrital components of the above-described volcaniclastic rocks were derived mostly from erosion and reworking of rocks composing sequences 1 and 2 within the sedimentary basin, and to a lesser extent from outside of the basin.

INFLUENCE OF THE DEPOSITIONAL ENVIRONMENT ON THE TUFF COMPOSITION, AND THEIR CORRELATORY POTENTIAL

The original source of the pyroclastic material, which is the main component of the tuffic horizons characterized in the previous sections, was the explosive activity of at least three volcanic cones that existed in the NE, central and SE regions of the Lublin Basin area at least since the Late Tournaisian. These operated in the area of the Lublin-Baltic early Carboniferous Igneous Province, and the rhyolitic nature of the tuffs indicates that the character of this province was not solely alkaline, as described by Poprawa et al. (2024). The composition of both lavas and tuffs indicates the bimodal – alkaline and acidic character of volcanism in the Lublin Basin during the Late Tournaisian and Late Visean (Waksmundzka et al., 2021; Kozłowska and Waksmundzka, 2023).

The presence of tuff 2.I in the NE and SE regions, which is the lowest one in sequence 2, indicates an intense explosive eruption that took place at the end of the RSL lowstand in this sequence. It seems that a volcano erupted in the NE region, as indicated by the presence of the coarse-ash fraction among the components of tuff 2.I (Radzyń IG 1 borehole; Fig. 7). This fraction fell to the ground surface relatively close to the volcanic cone, at a maximum distance of ~20–30 km or closer (cf. Francis and Oppenheimer, 2004). By contrast, the fine-ash fraction can be transported in air over considerable distances before deposition. Subsequently, the pyroclastic material was deposited in various environments that existed in the Lublin Basin at that time. In most areas of the NE and SE regions, tuff 2.I was deposited on the fluvial floodplain, covering it with a thick layer that could reach ~22 m in thickness (Korczmin IG 1 borehole). The rapid delivery of large amounts of pyroclastic material can strongly modify fluvial and lake sedimentary environments (cf. Di Capua and Scasso, 2019). However, in this case, after some time, the deposition of facies typical of the floodplain returned due to the RSL rising.

A calm, terrestrial depositional environment of the pyroclastic material, without the influence of erosional processes, contributed to its behaviour over much of the basin, and affected its colour and petrographic-mineralogical composition. The characteristic mottled yellow, red and beige colours of the first type of tuff 2.I indicate a terrestrial environment favouring intense kaolinitization and oxidation of iron compounds (Kościówko and Kural, 1982). Kaolinitization could have probably occurred in the pyroclastic material under the influence of hydrothermal processes and hypergene weathering in a tropical climate. After the tuff was overlain by the sediments of a transgressing sea, alteration continued under diagenetic conditions.

The second type of tuff 2.I, which is characterized by a dark grey or green-grey colour and contains bioclasts, was deposited across the rest of the NE (Fig. 7) and SE (Fig. 9) regions, in a marine environment: a shallow clay shelf and a prodelta. The colour of the tuffs indicates a less oxygenated sedimentary environment, in which kaolinitization and iron oxidation occurred less intensely (Kościówko and Kural, 1982). The conditions were also less favourable for tuff preservation due to the erosive action of waves and sea currents that partly washed out the deposited pyroclastic material and partly reworked and enriched it in the remains of marine organisms. Possibly for this reason, tuff 2.I has a relatively small thickness of ~ 2.5 metres here.

Another massive explosive eruption, which resulted in the deposition of tuff 2.II in the central (Fig. 8) and SE (Fig. 9) regions, took place during the RSL highstand of sequence 2. Inferring from the variability of the original thickness of the tuff, which can be up to ~30 m (Glinnik 2 borehole), a volcano in the central region or from the SE region could have been the source of this eruption. At that time, there was a fluvial floodplain in the central area of the Lublin Basin, which farther to the SE graded into a delta plain, the submarine part of a shallow-water delta, and then into a shallow carbonate and clay shelf. The pyroclastic material, like that of tuff 2.I, found its most favourable conditions for both preservation and kaolinitization in the calm, terrestrial environment of a fluvial floodplain, without any influence of erosional processes (Nasutów 2, Glinnik 2 and Nasutów 1 boreholes). However, in the central (Ciecierzyn 1, Świdnik 14 boreholes) and SE (Marynin 1, Ruskie Piaski IG 2, Zubowice IG 5 boreholes) regions, tuff horizon 2.II was evidently subjected to post-depositional erosional reduction during a forced regression and RSL lowstand of sequence 3.

The youngest tuff horizon 3.I in the studied section (Figs. 7 and 8) was deposited during a transgressive rise of RSL of sequence 3. Explosive eruption presumably took place in the NE (coarse-ash tuff in the Radzyń IG 1 borehole), and the pyroclastic material was deposited in the NE and central regions, mainly on an extensive area of prodelta and shallow clay shelf, and on a small area of fluvial floodplain. In the central region (Glinnik 1 borehole), tuff 3.I reached its greatest original thickness of ~40 m, suggesting that this eruption may have been the most massive, compared to previous ones. Tuff 3.I shows varied colours, i.e., mottled, creamy, red and yellow colours indicating an environment conducive to kaolinitization and iron oxidation, as well as grey and green colours indicating less favourable conditions (Kościówko and Kural, 1982). This is also reflected in the mineralogical composition of tuff 3.I, in which, unlike in the tuffs of sequence 2, kaolinite alone does not dominate, but occurs accompanied by berthierine that crystallizes using reduced iron (Fe^{2+}) of volcanic origin in shallow marine environments (Odin, 1988).

The present-day mineralogical composition of tuffs 2.I and 2.II of sequence 2, as well as of tuff 3.I of sequence 3, was influenced mainly by the rhyolitic type of pyroclastic material (Osborn et al., 1994), indicating acidic volcanism in the Lublin Basin in the Late Visean, in contrast to the Tournaisian deposits of sequence 1, which host volcanic rocks being products of both alkaline and acidic volcanism (Waksmundzka et al., 2021; Kozłowska and Waksmundzka, 2023).

A number of factors also had a fundamental impact, i.e. sedimentary environment, its oxygenation, and hydrothermal, weathering and diagenetic processes. According to the current state of knowledge suggesting that the Tournaisian deposits are the oldest in the Lublin Basin, no manifestations of proven alkaline volcanism have been so far recognized within the Upper Visean deposits, but only acidic volcanism. This issue requires further research, as $^{40}Ar/^{39}Ar$ dating indicates the possibility of alkaline volcanism also occurring in the Middle Visean (Pańczyk and Nawrocki, 2015). Due to the coarse tuff fraction, considerable thickness and regional nature of tuff horizons, it seems that the main source of pyroclastic material was in the NE region of the Lublin Basin, and not outside it, as suggested by Poprawa et al. (2024).

DIAGENETIC HISTORY

After deposition, the volcanic material in the sediment was transformed by hydrothermal, weathering and diagenetic processes (Fisher and Schmincke, 1984). Volcanic glass is thermodynamically unstable and is easily recrystallized. Reaction with water results in the release of ions, silica and aluminum into the pore solutions.

In the rocks studied, the main products of volcanic glass transformation are clay minerals. The dominant clay mineral is kaolinite, which forms at low temperatures (25–50°C) from acidic volcanic rocks (Osborn et al., 1994). Its formation involves the supply of H^+ and the removal of K^+ from the system in which the reaction takes place (Bjørlykke, 1989). Kaolinite, as a product of rhyolitic glass transformation, is formed at an early stage of diagenesis. Higher weathering intensity (Liu et al., 2022), as well as post-sedimentation circulation of hydrothermal fluids can lead to recrystallization of kaolinite, and thus to better ordering. Conversely, redeposition and transport decreases kaolinite ordering (Zadvernyuk et al., 2021). These effects may be seen through variations of the Hinckley Index measured for kaolinites in the samples studied (Table 5).

Berthierine also formed in the rocks at the early stages of diagenesis in a temperature range of 25–45°C (Hornibrook and Longstaffe, 1996). It crystallizes, using reduced iron (Fe^{2+}) of volcanic origin, in the methanogenic zone under conditions of very slow sedimentation (Odin, 1988). Its formation is related to a low activity of silica in solution, as kaolinite would otherwise precipitate (Toth and Fritz, 1997). Berthierine has also been found in nonmarine sediments: mostly laterites (Toth and Fritz, 1997), floodplains and estuarine/deltaic sediments (Taylor, 1990; Hornibrook and Longstaffe, 1996). During diagenesis, berthierine undergoes polymorphic alteration into chamosite (chlorite) in temperatures of ~70°C (Jahren and Aagaard, 1989; Hornibrook and Longstaffe, 1996) or it can be replaced by siderite (Morad, 1998).

At the early stage of diagenesis, siderite crystallized. Spherulitic forms of siderite indicate that it formed before mechanical compaction intensified. It crystallizes under hypoxic conditions, at low concentrations of dissolved sulphates, in sediments rich in reactive iron-rich minerals (Morad, 1998). Early diagenetic spherulitic siderite in the tuffs contains > 90% mol. $FeCO_3$. Syderoplesite precipitated from magnesium-enriched pore solutions circulating within volcaniclastic sandy and gravelly sediments.

Locally, pyrite crystallized. Its formation requires that the amount of H_2S produced by sulphate-reducing bacteria is higher than that of reduced iron (Postma, 1982). It is a post-depositional mineral because it fills voids inside bioclasts and forms concentrations in the form of laminae, lenses and irregular forms.

Feldspar grains were being dissolved under acidic conditions, taking up H^+ from pore solutions and releasing K^+ and Na^+. Secondary silica was precipitated in the form of chalcedony. This is shown by the observed effects of argillitization, albitization, and replacement by calcite.

Over time, the pH of pore solutions may have changed from acidic to alkaline. Calcite crystallized from calcium-containing pore solutions, which could have originated from dissolution of volcaniclastic detrital grains or calcium-rich plagioclases

(Milliken, 1989; Morad, 1989). Mixed-layered illite/smectite minerals and illite, which in places predominate over kaolinite, formed probably under such conditions. The illite content of >75% in mixed-layered illite/smectite minerals indicates that they could have formed from smectite at a temperature of ~120°C (Środoń, 1996), although lower temperatures of 70–90°C can be also suggested (Derkowski et al., 2020). These minerals can also form by illitization of kaolinite during burial, with the simultaneous bonding of potassium derived from dissolution of potassium feldspars (Huggett, 2005).

Anatase is a primary mineral, or is precipitated from solutions enriched in titanium ions, which were released likely from volcanic glass. Altered volcanic glass usually contains also high concentrations of phosphorus, which could be a source for apatite crystallization. Possibly, the apatite may also be related to bioclasts, the shells of which contain phosphorus, found in some tuffs. Local enrichment of the fluids in rare earth elements brought about the formation of carbonates containing mainly lanthanum and neodymium and smaller amounts of cerium, praseodymium and yttrium. The presence of volcaniclastic rocks enriched in rare earth elements in the SE region indicates a mineral resource potential of the deposits in sequence 2, which should be examined further. Such research should also cover the remaining sequences 1 and 3, 4, which are part of the Kłodnica Member, in which volcanic, pyroclastic and volcaniclastic rocks occur in abundance.

CONCLUSIONS

1. The feasibility of correlating the tuffs between different areas of the Lublin Basin indicates their regional nature, and thus they can be considered as good correlation horizons, here marked by the symbols 2.I, 2.II and 3.I.

2. There are two tuffic horizons within sequence 2. In the NE and SE regions, the lower tuffic horizon 2.I is found at the top of LST deposits. It directly overlies sandstones and volcaniclastic conglomerates of fluvial channels or co-occurs with fluvial floodplain lithofacies. In the central and SE regions, the upper tuffic horizon 2.II is encountered within the HST deposits. It was deposited in various environments, on a fluvial floodplain, deltaic plain, prodelta, shallow clay-dominated shelf, and shallow carbonate shelf.

3. The basic petrographic-mineralogical compositions of tuffs 2.I and 2.II of sequence 2 are generally similar, and the observed differences lie in the details. These are fine-ash vitric and vitric-crystal tuffs, occasionally coarse-ash vitric tuffs. The main clay mineral is kaolinite, the amount of which can exceed 80%. Illite and mixed-layered illite/smectite minerals are also present. Carbonate minerals are represented by siderite, sideroplesite and calcite. Hematite is found in greater amounts in tuffs from the NE and central regions, while greater accumulations of pyrite and jarosite were encountered in tuffs from the SE region.

4. Another tuffic horizon 3.I within the TST of sequence 3 in the NE and central regions is associated with the sediments of fluvial floodplain and of prodelta of a shallow-water delta. It is represented by fine-ash vitric tuffs and coarse-ash vitric-lithic tuffs. In the NE region, the predominant clay mineral is kaolinite, accompanied in places by serpentine – berthierine, while in the central region, mixed-layered illite/smectite and illite minerals predominate. The common minerals are anatase and, among carbonate minerals, siderite, sideroplesite and Fe/Mn-calcite. Hematite is found in the NE region.

5. The source of rhyolitic pyroclastic material for the deposition of the tuffic horizons was the explosive acidic volcanic activity that took place in the Lublin Basin in the Late Visean. The present-day mineralogical composition of the tuffs results from the type of pyroclastic material and from a number of factors that affected it after deposition. The most favourable environment for the preservation of the tuffs and for the intense kaolinitization and oxidation of iron compounds during hypergene weathering in a tropical climate was the terrestrial environment of a fluvial floodplain. Other factors included hydrothermal and diagenetic processes that interacted with the pyroclastic material for the longest time and affected its alteration the most.

6. Deposition of fine-grained and very fine-grained volcaniclastic polymictic orthoconglomerates (sequence 2 in the NE and SW regions) and volcaniclastic sandstones (quartz wackes, sublithic and lithic arenites) (sequence 2 in the NE, central and SE regions) that fill the river channels and incised valleys was preceded by bedrock erosion in the sedimentary basin hosting the deposits of sequences 1 and 2. Detrital components of the volcaniclastic rocks, therefore, were derived mostly from erosion and reworking of deposits of older sequences, and to a lesser extent from outside of the basin.

7. The study of tuffs and volcaniclastic rocks occurring in the Upper Visean deposits of sequences 2 and 3 is important not only from a scientific, but also from a utilitarian point of view. A preliminary estimate shows that the Al_2O_3 content in tuffic horizons 2.I, 2.II and 3.I from the NE and central regions of the Lublin Basin can reach ~28–35%, which is a prospective amount for refractory raw materials. Enrichment in rare earth elements (carbonates containing lanthanum and neodymium) was also encountered in the volcaniclastic rocks of sequence 2 from the SE region of the Lublin Basin.

Acknowledgements. The authors would like to thank the reviewers: Prof. S. Skompski and an anonymous reviewer for their insightful comments and remarks which allowed us to improve our manuscript. The editor of Geological Quarterly, Prof. A. Wysocka, is also warmly acknowledged for helpful suggestions. The research was carried out at the Polish Geological Institute - National Research Institute and financed by the Ministry of Science and Higher Education (61.2805.1705.00.0, 62.9012.2045.00.0).

REFERENCES

Baldwin, B., Butler, C.O., 1985. Compaction curves. AAPG Bulletin, **69**: 622–626; https://doi.org/10.1306/AD462547-16F7-11D7-8645000102C1865D

Bjørlykke, K., 1989. Sedimentology and Petroleum Geology. Springer, Berlin.

Bolewski A., 1982. Mineralogia szczegółowa (in Polish). Wydaw. Geol., Warszawa.

Carrillo, U., Díaz-Villanueva, V., 2021. Impacts of volcanic eruptions and early recovery in freshwater environments and organisms. Biological Reviews, **96**: 2546–2560; https://doi.org/10.1111/brv.12766

Cebulak, S., 1978. Bauxite and kaolinite raw materials in the Lublin Coal Basin (in Polish with English summary). Przegląd Geologiczny, **26**: 542–545.

Cebulak, S., 1988a. Petrographic characteristics of Carboniferous deposits (in Polish with English summary). Prace Instytutu Geologicznego, **122**: 77–88.

Cebulak, S., 1988b. Geological outline of sub-Carboniferous basement (in Polish with English summary). Prace Instytutu Geologicznego, **122**: 31–34.

Cebulak, S., Porzycki, J., 1966. Lithological-petrographic characteristics of the deposits of the Lublin Carboniferous (in Polish with English summary). Prace Instytutu Geologicznego, **44**: 21–47.

Cebulak, S., Porzycki, J., Laskowski, M., Różkowski, A., Rudzińska, T., Szewczyk, J., Karwasiecka, M., Waksmundzka, M.I., 2011. Badania surowcowe boksytów i węgli występujących w utworach karbonu (in Polish). Profile Głębokich Otworów Wiertniczych Państwowego Instytutu Geologicznego, **130**: 116–122.

Depciuch, T., 1974. Rocks of the Precambrian Platform in Poland (in Polish with English summary). Prace Instytutu Geologicznego, **74**: 81–83.

Derkowski, A., Środoń, J., Goryl, M., Marynowski, L., Szczerba, M., Mazur, S., 2021. Long-distance fluid migration defines the diagenetic history of unique Ediacaran sediments in the East European Craton. Basin Research, **33**: 570–593; https://doi.org/10.1111/bre.12485

Di Capua, A., Scasso, R.A., 2020. Sedimentological and petrographic evolution of a fluviolacustrine environment during the onset of volcanism: volcanically-induced forcing of sedimentation and environmental responses. Sedimentology, **67**: 1879–1913; https://doi.org/10.1111/sed.12681

Falini, G., Foresti, E., Gazzano, M., Gualtieri, A.F., Leoni, M., Lesci, I.G., Roveri, N., 2004. Tubular-shaped stoichiometric chrysotile nanocrystals. Chemistry, A European Journal, **10**: 3043–3049; https://doi.org/10.1002/chem.200305685

Fisher, R.V., Schmincke, H.-U.,1984. Pyroclastic Rocks. Springer, Berlin; https://doi.org/10.1007/978-3-642-74864-6

Flügel, E., 2004. Microfacies of Carbonate Rocks Analysis, Interpretation and Application. Springer; https://doi.org/10.1017/S0016756806221940

Francis, P., Oppenheimer, C., 2004. Volcanoes. Oxford University Press, Oxford.

Franks, S.G., Zwingmann, H., 2010. Origin and timing of late diagenetic illite in the Permian–Carboniferous Unayzah sandstone reservoirs of Saudi Arabia. AAPG Bulletin, **94**: 1133–1159; https://doi.org/10.1306/04211009142

Grocholski, A., Ryka, W., 1995. Carboniferous magmatism of Poland. Prace Państwowego Instytutu Geologicznego, **148**: 181–190.

Hornibrook, E.R., Longstaffe, F.J., 1996. Berthierine from the lower cretaceous Clearwater formation, Alberta, Canada. Clays and Clay Minerals, **44**: 1–21; https://doi.org/10.1346/CCMN.1996.0440101

Huggett, J.M., 2005. Sedimentary rocks / Clays and their diagenesis. Encyclopedia of Geology, 62–70; https://doi.org/10.1016/B0-12-369396-9/00311-7

Jackowicz, E., 1985. Charakterystyka skał wulkanicznych i magmowych kompleksu dewońsko-karbońskiego (in Polish). Inw. 34332. CAG PIG-PIB, Warszawa.

Jahren, J.S., Aagaard, P., 1989. Compositional variations in diagenetic chlorites and illites, and relationships with formation-water chemistry. Clay Minerals, **24**: 157–170; https://doi.org/10.1180/claymin.1989.024.2.04

Jaworowski, K., 1987. Petrographic canon of the most common sedimentary rocks (in Polish). Przegląd Geologiczny, **35**: 205–209.

Kasiński, J., 2023. Opisy basenów. Baseny mezo-kenozoiczne pozakarpackie. Paleogeńsko-neogeński basen Niżu Polskiego (in Polish). Prace Państwowego Instytutu Geologicznego, **207**: 69–70; https://www.pgi.gov.pl/oferta-inst/wydawnictwa/serie-wydawnicze/prace-pig/14201-prace-pig-tom-207-2023.html

Kmiecik, H., 1988. Miospore stratigraphy of the Carboniferous deposits (in Polish with English summary). Prace Instytutu Geologicznego, **122**: 131–141; 235–237.

Kościówko, H., Kural, S., 1982. Występowanie surowców kaolinitowych na Dolnym Śląsku. Klasyfikacja i geneza (in Polish). In: Surowce kaolinitowe. Monografie surowców mineralnych Polski (ed. H. Leszczyszyn): 25–33. Wydaw. Geol., Warszawa.

Kozłowska, A., 2023. Wyniki badań petrograficznych utworów karbonu (in Polish). Profile Głębokich Otworów Wiertniczych Państwowego Instytutu Geologicznego, **167**: 126–147.

Kozłowska, A., Popek, T., 2018. Petrologia utworów karbonu (in Polish). Profile Głębokich Otworów Wiertniczych Państwowego Instytutu Geologicznego, **149**: 65–71.

Kozłowska, A., Waksmundzka, M.I., 2020. Diagenesis, sequence stratigraphy and reservoir quality of the Carboniferous deposits of the southeastern Lublin Basin (SE Poland). Geological Quarterly, **64**: 422–459; https://doi.org/10.7306/gq.1532

Kozłowska, A., Waksmundzka, M.I., 2023. Petrographic-mineralogical characteristics of the new tuff horizons with associated volcanoclastic conglomerates and sandstones from the Kłodnica Member (Tournaisian, Visean) in the Lublin Basin (in Polish with English summary). Przegląd Geologiczny, **71**: 207–211; https://doi.org/10.7306/2023.15

Krzemiński, L., 1999. Anorogenic Carboniferous sandstones from the northwestern border of the Holy Cross Mountains, Central Poland (in Polish with English summary). Przegląd Geologiczny, **47**: 978–986.

Lander, R.H., Bonnell, L.M., 2010. A model for fibrous illite nucleation and growth in sandstones. AAPG Bulletin, **94**: 1161–1187; https://doi.org/10.1306/04211009121

Le Maitre, R.W., Streckeisen, A., Zanettin, B., Le Bas, M.J., Bonin, B., P. Bateman, P., 2002. Igneous rocks. A classification and glossary of terms, **2**. Cambridge University Press; https://doi.org/10.1017/CBO9780511535581

Leszczyński, K., 2023. Opisy basenów. Baseny mezo-kenozoiczne pozakarpackie. Mezozoiczny basen Niżu Polskiego (in Polish). Prace Państwowego Instytutu Geologicznego, **207**: 64–65; https://www.pgi.gov.pl/oferta-inst/wydawnictwa/serie-wydawnicze/prace-pig/14201-prace-pig-tom-207-2023.html

Liu, D., Zhang, Y., Zhou, A., Nnachi, E.N., Huo, S., Zhang, Q., 2022. The kaolinite crystallinity and influence factors of coal-measure kaolinite rock from Datong Coalfield, China. Minerals, **12**, 54; https://doi.org/10.3390/min12010054

Martinsen, O.J., 1994. Evolution of an incised-valley fill, the Pine Ridge Sandstone of Southeastern Wyoming, U.S.A.: systematic sedimentary response to relative sea-level change. SEPM Special Publication, **51**: 109–128; https://doi.org/10.2110/pec.94.12.0109

Miall, A.D., 1977. A review of the braided-river depositional environment. Earth-Science Reviews, **13**: 1–62; https://doi.org/10.1016/0012-8252(77)90055-1

Miall, A.D., 1978. Lithofacies types and vertical profile models in braided river deposits: a summary. Canadian Society of Petroleum Geologists Memoir, **5**: 597–604.

Migier, T., 1988. Macrofloral stratigraphy of the Carboniferous deposits (In Polish with English summary). Prace Instytutu Geologicznego, **122**, 120–131; 234–235.

Michum, Jr R.M., 1977. Seismic stratigraphy and global changes of sea level, **1**: Glossary of terms used in seismic stratigraphy. AAPG Memoir, **26**: 205–212; https://doi.org/10.1016/0012-8252(77)90055-1

Migaszewski, Z., 1995. Occurrence of pyroclastic rocks in the Lower Carboniferous of the Holy Cross Mts (Central Poland) (in Polish with English summary). Przegląd Geologiczny, **43**: 7–10.

Milliken, K.L., 1998. Carbonate diagenesis in non-marine foreland sandstones at the western edge of the Alleghanian overthrust belt, Southern Appalachians. IAS Special Publication, **26**: 87–105; https://doi.org/10.1002/9781444304893.ch4

Morad, S., 1998. Carbonate cementation in sandstones: distribution patterns and geochemical evolution. IAS Special Publication, **26**: 1–26; https://doi.org/10.1002/9781444304893.ch1

Musiał, Ł., Tabor, M., 1979. Stratygrafia karbonu Lubelskiego Zagłębia Węglowego na podstawie makrofauny (in Polish). In: Stratygrafia Węglonośnej Formacji Karbońskiej w Polsce (ed. T. Migier). II Sympozjum Sosnowiec. Wydaw. Geol., Warszawa. 35–43.

Musiał, Ł., Tabor, M., 1988. Macrofaunal stratigraphy of Carboniferous (in Polish with English summary). Prace Instytutu Geologicznego, **122**: 88–122, 232–233.

Muszyński, A., Biernacka, J., Lorenc, S., Protas, A., Urbanek, Z., Wojewoda, J., 1996. Petrology and a depositional environment of Lower Carboniferous rocks near Dygowo and Kłanino (the Koszalin-Chojnice Zone) (in Polish with English summary). Geologos, **1**: 93–126.

Nadon, G.C., 1994. The genesis and recognition of anastomosed fluvial deposits: data from the St. Mary River Formation, southwestern Alberta, Canada. Journal of Sedimentary Research, **B64**: 451–463; https://doi.org/10.1306/D4267FE1-2B26-11D7-8648000102C1865D

Narkiewicz, M., 2007. Development and inversion of Devonian and Carboniferous basins in the eastern part of the Variscan foreland (Poland). Geological Quarterly, **51** (3): 231–256; https://gq.pgi.gov.pl/article/view/7453

Narkiewicz, M., 2023. Opisy basenów. Baseny eksternidów waryscyjskich i przedpola waryscydów. Dewoński basen lubelski (in Polish). Prace Państwowego Instytutu Geologicznego, **207**: 30–31; https://www.pgi.gov.pl/oferta-inst/wydawnictwa/serie-wydawnicze/prace-pig/14201-prace-pig-tom-207-2023.html

Odin, G.S., 1988. The verdine facies from the lagoon of New Caledonia. Developments in Sedimentology, **45**: 57–82; https://doi.org/10.1016/S0070-4571(08)70059-1

Osborne, M., Haszeldine, R.S., Fallick, A.E., 1994. Variation in kaolinite morphology with growth temperature in isotopically mixed pore-fluids, Brent Group, UK North Sea. Clay Minerals, **29**: 591–608; https://doi.org/10.1180/claymin.1994.029.4.15

Pańczyk, M., Nawrocki, J., 2015. Tournaisian $^{40}Ar/^{39}Ar$ age from alkaline basalts from the Lublin Basin (SE Poland). Geological Quarterly, **59** (3): 473–478; https://doi.org/10.7306/gq.1218

Peryt, T.M., 2023. Opisy basenów. Baseny permskie. Polski basen cechsztyński (in Polish). Prace Państwowego Instytutu Geologicznego, **207**: 60–61; https://www.pgi.gov.pl/oferta-inst/wydawnictwa/serie-wydawnicze/prace-pig/14201-prace-pig-tom-207-2023.html

Pettijohn, F. J., Potter, P. E., Siever, R., 1972. Sand and Sandstone. Springer, New York; https://doi.org/10.1007/978-1-4612-1066-5

Pointon, M.A., Chew, D.M., Delcambre, B., Sevastopulo, G.D., 2018. Geochemistry and origin of Carboniferous (Mississippian; Viséan) bentonites in the Namur-Dinant Basin, Belgium: evidence for a Variscan volcanic source. Geologica Belgica, **21**: 1–17; https://doi.org/10.20341/GB.2017.011

Popek, T., 1986. Traces of volcanic activity in the Upper Visean in the Lublin region (in Polish with English summary). Przegląd Geologiczny, **34**: 212–215.

Poprawa, P., Nejbert, K., Krzywiec, P., Krzemińska, E., Krzemiński, L., Mazur, S., Słaby, E., 2024. Alkaline magmatism from the Lublin-Baltic area of Poland (SW slope of the East European Craton) – manifestation of hitherto unrecognized early Carboniferous igneous province. Terra Nova, **36**: 77–88; https://doi.org/10.1111/ter.12681

Porzycki, J., 1979. Litostratygrafia osadów karbonu Lubelskiego Zagłębia Węglowego (in Polish). In: Stratygrafia węglonośnej formacji karbońskiej w Polsce (ed. T. Migier): 19–27. II Sympozjum, Sosnowiec. Wydaw. Geol., Warszawa.

Porzycki, J., 1988. History of geological survey and discovery of the Lublin Coal Basin. Lithologic and sedimentologic characteristics of Carboniferious deposits (in Polish with English summary). Prace Instytutu Geologicznego, **122**: 9–17, 40–76.

Porzycki, J., Zdanowski, A., 1995. Southeastern Poland (Lublin Carboniferous Basin). Prace Państwowego Instytutu Geologicznego,**168**: 102–109.

Postma, D., 1982. Pyrite and siderite formation in brackish and freshwater swamp sediments. American Journal of Science, **282**: 1151–1183; https://doi.org/10.2475/AJS.282.8.1151

Reading, H.G., 1978. Facies. In: Sedimentary Environments and Facies (ed. H.G. Reading): 4–14. Blackwell; https://doi.org/10.1002/esp.3290060116

Rust, B.R., 1978. A classification of alluvial channel systems. Canadian Society of Petroleum Geologists Memoir, **5**: 187–198.

Rust, B.R., 1984. Proximal braidplain deposits in the Middle Devonian Malbaie Formation of eastern Gaspé, Quebec, Canada. Sedimentology, **31**: 675–695; https://doi.org/10.1111/j.1365-3091.1984.tb01230.x

Ryka, W., Maliszewska, A., 1991. Słownik petrograficzny (in Polish). 2nd edition. Wydaw. Geol., Warszawa.

Simon, C., Stephan, J., Gwenael, J., Camoin, G., Boudagher-Fadel, M.K., Bachčlery, P., Caline, B., Boichard, R., Sidonie, R., Yannick, T., Estelle, T., Charline, G., 2017. Impact of tectonic and volcanism on the Neogene evolution of isolated carbonate platforms (SW Indian Ocean). Sedimentary Geology, **355**: 114–131; https://doi.org/10.1016/j.sedgeo.2017.04.008

Skompski, S., 1988. Limestone microfacies and facies position of Upper Visean sediments in north-eastern part of the Lublin Coal Basin (In Polish with English summary). Przegląd Geologiczny, **36**: 25–30.

Skompski, S., 1995a. Tectonic framework and development of sedimentation at the margin of the East European Platform. In: XIII International Congress on Carboniferous-Permian (XIII ICC-P), Kraków, Guide to Excursion A2: 5–9.

Skompski, S., 1995b. Succession of limestone microfacies as a key to the origin of the Yoredale-type cyclicity (Viséan/Namurian, Lublin Basin, Poland). In: XIII International Congress on Carboniferous-Permian (XIII ICC-P), Kraków, Abstract: 133.

Skompski, S., 1996. Stratigraphic position and facies significance of the limestone bands in the subsurface Carboniferous succession of the Lublin Upland. Acta Geologica Polonica, **46**: 171–268.

Skompski, S., Soboń-Podgórska, J., 1980. Foraminifers and conodonts in the Viséan deposits of the Lublin Upland. Acta Geologica Polonica, **30**: 87–96.

Soboń-Podgórska, J., 1988. Microfaunal stratigraphy of the Carboniferous deposits (foraminifers) (in Polish with English summary). Prace Instytutu Geologicznego, **122**: 112–120; 233–234.

Soboń-Podgórska, J., Tomaś, A. 1995. Foraminifera. Prace Państwowego Instytutu Geologicznego, **148**: 44–47.

Svendsen, J., Stollhofen, H., Krapf, C.B.E, Stanistreet, I.G., 2003. Mass and hyperconcentrated flow deposits record dune damming and catastrophic breakthrough of ephemeral rivers, Skeleton Coast Erg, Namibia. Sedimentary Geology, **160:** 7–31; https://doi.org/10.1016/S0037-0738(02)00334-2

Szczerba, J., 2006. Klasyfikacja materiałów ogniotrwałych według zunifikowanych norm unijnych (in Polish). Materiały Ceramiczne, **58**: 6–16; https://www.researchgate.net/publication/279646194

Środoń, J., 1996. Clay minerals in diagenetic processes (in Polish with English summary). Przegląd Geologiczny, **44**: 604–607.

Taylor, K.G., 1990. Berthierine from the non-marine Wealden (Early Cretaceous) sediments of south-east England. Clay Minerals, **25**: 391–399; https://doi.org/10.1180/claymin.1990.025.3.13

Tomaszczyk, M., Jarosiński, M., 2017. The Kock Fault Zone as an indicator of tectonic stress regime changes at the margin of the East European Craton (Poland). Geological Quarterly, **61** (4): 908–925; https://doi.org/10.7306/gq.1380

Toth, T.A., Fritz, S.J., 1997. An Fe-berthierine from a cretaceous laterite: Part I. Characterization. Clays and Clay Minerals, **45**: 564–579; https://doi.org/10.1346/CCMN.1997.0450408

Vail, P.R., Todd, R.G. 1981. Northern North Sea Jurassic unconformities, chronostratigraphy and sea-level changes from seismic stratigraphy. In: Petroleum Geology of the Continental Shelf of North West Europe (eds. L.V. Illing and G.D. Hobson): 216–235. Heyden, London; https://doi.org/10.1086/628731

Van Wagoner, J.C., 1985. Reservoir facies distribution as controlled by sea-level change. Society of Economic Paleontologists and Mineralogists Mid-Year Meeting Abstracts, Golden, Colorado: 91–92.

Waksmundzka, M.I., 1998. Depositional architecture of the Carboniferous Lublin Basin (in Polish with English summary). Prace Państwowego Instytutu Geologicznego, **165**: 89–100.

Waksmundzka, M.I., 2008. Correlation and origin of the Carboniferous sandstones in the light of sequence stratigraphy and their hydrocarbon potential in the NW and Central parts of the Lublin Basin (in Polish with English summary). Biuletyn Państwowego Instytutu Geologicznego, **429**: 215–224.

Waksmundzka, M.I., 2010. Sequence stratigraphy of Carboniferous paralic deposits in the Lublin Basin (SE Poland). Acta Geologica Polonica, **60**: 557–597.

Waksmundzka, M.I., 2012. Braided-river and hyperconcentrated-flow deposits from the Carboniferous of the Lublin Basin (SE Poland) – a sedimentological study of core data. Geologos, **18:** 135–161; https://doi.org/10.2478/v10118-012-0008-y

Waksmundzka, M.I., 2013. Carboniferous coarsening-upward and non-gradational cyclothems in the Lublin Basin (SE Poland): palaeoclimatic implications. Geological Society Special Publications, **376**: 141–175; https://doi.org/10.1144/SP376.18

Waksmundzka, M.I., Buła, Z., 2020. Geological Map of Poland without Cenozoic, Mesozoic and Permian deposits 1:2,500,000. In: Geological Atlas of Poland (eds. J. Nawrocki and A. Becker): 28–29. PGI – NRI, Warsaw.

Waksmundzka, M.I., Kozłowska, A., Pańczyk, M., 2021. A putative Tournaisian and Visean volcanic-sedimentary succession in the Lublin Basin, SE Poland: depositional processes, petrological characteristics and sequence stratigraphy. Acta Geologica Polonica, **71**: 305–344; https://doi.org/10.24425/agp.2020.134559

Walker, R.G., 1992. Facies, facies models, and modern stratigraphic concepts. In: Facies Models: Response to Sea Level Change (eds. R.G. Walker and N.P. James): 1–14. Geological Association of Canada, St. Johns; https://doi.org/10.1002/gj.3350290317

Zadvernyuk, H., Kadoshnikov, V., Shekhunova, S., Remez, S., 2021. Particle size distribution and crystallinity as indicators of kaolinite genesis. Applied Clay Science, **213**, 106236; https://doi.org/10.1016/j.clay.2021.106236

Zieliński, T., 1992a. Marginal moraines of NE Poland – sediments and depositional conditions (in Polish with English summary). Prace Naukowe Uniwersytetu Śląskiego, **1325**: 7–95.

Zieliński, T., 1992b. Proglacial valleys facies of the Silesian Upland – genetic factors and their sedimentological effects. Geologia Sudetica, **26**: 83–118.

Zieliński, T., 1995. Kod litofacjalny i litogenetyczny – konstrukcja i zastosowanie (in Polish). In: Badania osadów czwartorzędowych, wybrane metody i interpretacja wyników (eds. E. Mycielska-Dowgiałło and J. Rutkowski): 220–235.

Żelichowski, A.M., 1969. Karbon (in Polish). In: Ropo- i gazonośność obszaru lubelskiego na tle budowy geologicznej – część I: Budowa geologiczna obszaru lubelskiego (ed. S. Depowski). Prace Geostrukturalne Instytutu Geologicznego, 70–85.

Żelichowski, A.M., 1972. Evolution of the geological structure of the area between the Góry Świętokrzyskie and the river Bug (in English with Polish summary). Biuletyn Instytutu Geologicznego, **263**: 7–97.